Journal of Materials Chemistry C

ROYAL SOCIETY OF CHEMISTRY

REVIEW

View Article Online
View Journal | View Issue

Cite this: J. Mater. Chem. C, 2022, 10, 13351

Transparent stretchable hydrogel sensors: materials, design and applications

Yinping Liu,†[a] Lulu Wang,†[a] Yuanyuan Mi,[a] Sisi Zhao,[a] Simeng Qi,[a] Meng Sun,[a] Bo Peng,[b] Quan Xu,[a] Yingchun Niu*[a] and Yang Zhou*[a]

Received 18th March 2022,
Accepted 16th April 2022

DOI: 10.1039/d2tc01104b

rsc.li/materials-c

Flexible sensors have great potential for human motion sensing, medical monitoring, electronic skin and display devices. Flexible hydrogel sensors with transparent characteristics have a good visual effect, which can be used for "invisible" devices and visual optical monitoring, as well as to improve the aesthetics of devices for daily usage, *etc.* However, there are no systematic reviews on the working principle, characteristics and application prospects of transparent stretchable hydrogel sensors. In this review, we summarize recent advances in wearable strain sensors, pressure sensors, temperature sensors, humidity sensors and gas sensors based on transparent stretchable hydrogels, emphasizing materials, designs and applications. We also discuss the combinations and applications of sensors with emerging technologies such as wearable devices, artificial intelligence, human–computer interaction and 3D printing. Finally, this review presents a brief summary, challenges, and perspectives of transparent stretchable hydrogel sensors.

1. Introduction

Flexible sensors attract extensive attention due to their portability,[1] mechanical robustness,[2] high flexibility[3] and great conformability,[4] which can transform external stimuli, such as strain,[5,6] pressure,[7,8] temperature,[9,10] and chemical substances,[11,12] into detectable signals (such as resistance,[13] color,[14] voltage,[15] capacitance[16]). A hydrogel is a kind of 3D cross-linked network composed of hydrophilic polymer chains with an aqueous-rich environment.[17,18] It has the advantages of simple preparation technology,[19] good biocompatibility,[20] high viscoelasticity[21] and unique stimulus-response characteristics.[22] Based on these advantages, flexible hydrogel sensors are showing tremendous potential in remote health monitoring,[23–26] wound healing,[27–30] drug delivery,[31,32] environmental monitoring,[33,34] human-machine interface,[35–37] intelligent robots[38–40] and other emerging fields.

Hydrogel sensors with transparent properties have the unique advantages of good visual effect, being able to be used for "invisible" equipment and visualizing optical monitoring, as well as improving the aesthetics of daily usage, which endows sensors with special applications, including in beautiful electronic skin,[41–44] wearable electronic devices,[45–48] touch screens for human-machine interaction,[49–51] *etc.*

Transparent hydrogel sensors are divided into wearable strain sensors,[52] pressure sensors,[53] temperature sensors,[54] humidity sensors[55] and gas sensors,[56] according to different applications (Fig. 1). The fundamental sensing principle of a wearable strain sensor is evaluated by its electrical resistance change when they deform greatly under external stimulation.[57] The pressure sensor rearranges the electrostatic potential of internal ions, causing changes in electrical resistance, which is based on the piezoresistive effect of the hydrogel.[58] The temperature sensor utilizes the monotonic increase of the electrical conductivity of the hydrogel with temperature to monitor the temperature change in real-time.[54]

[a] State Key Laboratory of Heavy Oil Processing Beijing Key Laboratory of Biogas Upgrading Utilization, China University of Petroleum-Beijing, Beijing 102249, China. E-mail: ycniu92@163.com, zhouyang@cup.edu.cn
[b] Department of Applied Physics, Aalto University, FIN-00076 Aalto, Finland
† Those authors contributed equally to this work.

Yang Zhou

Yang Zhou is now an Assistant Professor in the College of New Energy and Materials Science, China University of Petroleum, Beijing (CUPB), China. He obtained his PhD, Master and Bachelor degrees from Nanyang Technological University, Singapore. His research interests include hydrogel based functional materials and stimuli-responsive materials, and their application in energy saving engineering and petroleum engineering fields.

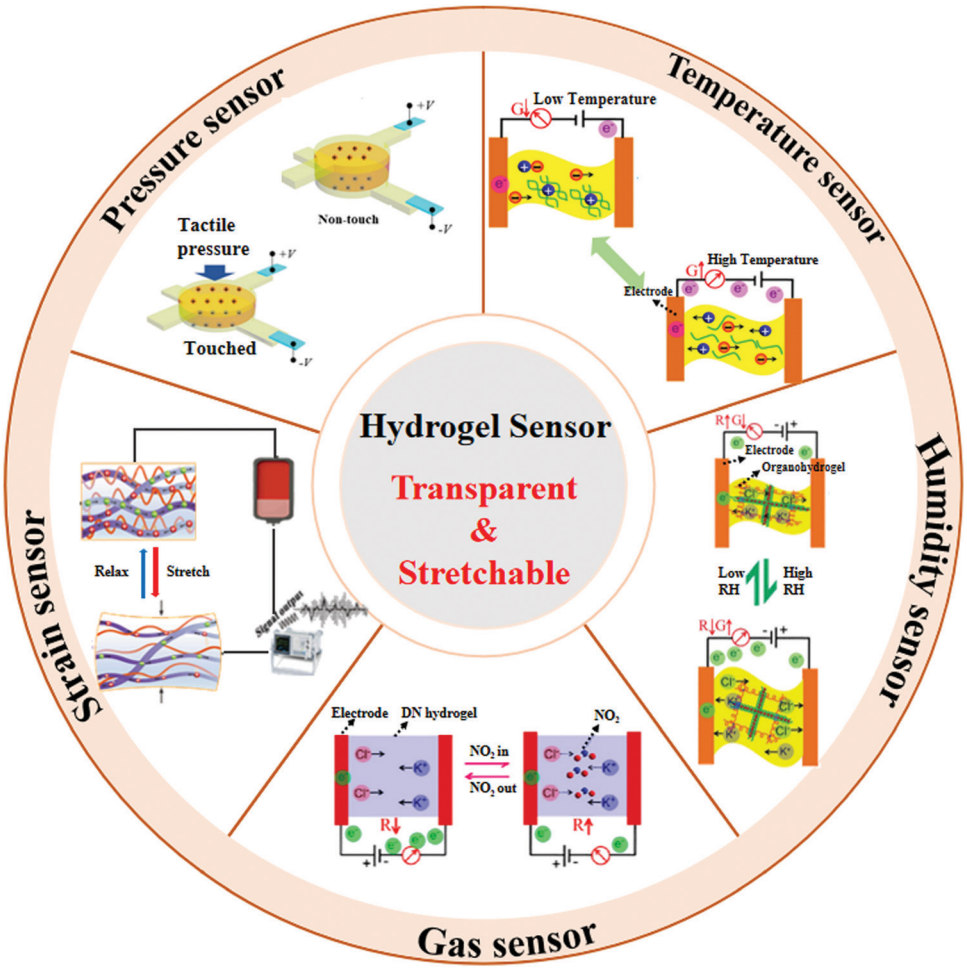

Fig. 1 Schematic diagram of the sensing mechanism of a wearable strain sensor, pressure sensor, temperature sensor, humidity sensor and gas sensor.

For the humidity hydrogel sensor, the hydrophilic groups on hydrogels/organohydrogels can absorb and desorb moisture from the surrounding environment upon relative humidity variations, which can change the electrical properties.[59] The gas sensor forms a certain adsorption-desorption process with the gases to be measured in the sensing process, which leads to the change of electrical resistance.[60] In addition to transparency and stretchability, sensors often have additional functions such as self-healing,[50] frost resistance,[61] dryness resistance,[62] adhesion,[63] *etc.*

In this review, we summarize recent developments in transparent stretchable hydrogel sensors, including wearable strain sensors, pressure sensors, temperature sensors, humidity sensors and gas sensors. Firstly, we summarize the advantages of sensors with transparent characteristics, simultaneously interpreting the mechanism and subclasses of different sensors. Secondly, the performance improvement strategies and demonstrations are discussed. The special structural design of hydrogel sensors is mentioned, including sandwich structure,[64–67] array structure,[68–70] kirigami structure[71] and woven structure.[72] Finally, strategies for the future improvement of transparent stretchable hydrogel sensors are summarized in the last section.

2. Transparent stretchable wearable strain sensors

Transparent stretchable wearable strain sensors are mainly composed of active materials and flexible substrates/matrices. The special network structure and high hydrophilicity enable these hydrogels to hold large amounts of water, confer high transparency, flexibility, stretchability, viscoelasticity, self-adhesiveness, good biocompatibility and even anti-microbial activity to hydrogels by using some particular polymers and polymer networks.[73,74] Therefore, the potential applications of transparent stretchable wearable strain sensors in various fields such as wearable devices, human-machine interface (HMI) systems, artificial electronic skin (e-skin), intelligent robotics, medical monitoring, and automation have received extensive attention. Common transparent hydrogel substrates include polyvinyl alcohol (PVA), polyacrylamide (PAM) and polyacrylic acid (PAA). We introduce wearable strain sensors based on transparent hydrogels through current commonly used elastic substrates.

2.1 Applications of human motion monitoring

The application of transparent hydrogel sensors to human monitoring systems has significant advantages. The optical

visualization effect of hydrogels enables the wider application of hydrogel sensors. Wearable flexible sensors based on transparent hydrogels can monitor various human movements such as pulse, throat, facial expressions, and joints. Although it's easy to measure these vital signals in the hospital, monitoring human motions noninvasively and continuously anywhere is challenging.

2.1.1 PVA-based. Polyvinyl alcohol (PVA) hydrogels have good transparency which has the potential to meet the appearance requirements of wearable human sensors. In addition, the principle of regional crystallization of PVA hydrogels at low temperatures improves their mechanical properties after freeze-thaw cycles, which further improves its mechanical strength. Previously, Zhang *et al.* added phytic acid (PA) to PVA hydrogels and obtained conductive hydrogels through freeze-thaw cycles.[75] This PVA-PA hydrogel has a maximum strain of 1100% and a transparency of 95%. The PVA-PA hydrogel was assembled into a wearable strain sensor capable of monitoring human motion and sending out a bluetooth signal through an integrated circuit (Fig. 2a). Based on PVA-PA hydrogels, real-time monitoring of human joint movement and health can be accomplished. Pan *et al.* designed a high-performance PVA/glycerol/NaCl (PGN) transparent hydrogel sensor.[76] Due to the synergistic effect of glycerol and sodium chloride, the freezing point of the water phase is effectively lowered and the frost resistance is improved. The sensor can stably monitor the electrochemical signal changes during wrist flexion at −20 °C (Fig. 2b). These rapid, stable, anti-freezing strain-sensitive PGN hydrogel sensors could provide more possibilities for wearable smart devices.

However, when the objects monitored are weak movements such as pulse, throat, facial smile, *etc.*, wearable electronic devices require extremely sensitive monitoring capabilities. Gang *et al.* developed a biocompatible, transparent stretchable sensor based on a binary networked conductive hydrogel of PVA and PAM.[77] Wearing the transparent hydrogel sensor in the human throat can distinguish the pronunciation of various english words such as ''sensor'' (Fig. 2c). The stable current patterns were similar when the same word was repeated three times. Distinct waveforms with characteristic peaks appeared for different words, which indicated the ability of the transparent sensor to recognize and recover speech.

2.1.2 PAM-Based. Polyacrylamide (PAM) hydrogels have wide application prospects in drug-controlled release,[78] material separation,[79] industry,[80] *etc.* Because the polyacrylamide structure contains an amide group, it is easy to form a hydrogen bond, so it can obtain a variety of modifiers with a branched-chain or network structure by grafting or cross-linking.[81] Inspired by fish, Xu *et al.* fabricated an anti-icing hydrogel sensor by incorporating antifreeze proteins into a chemically crosslinked network of acrylamide and 2-acrylamide-2-methylpropanesulfonic acid copolymers.[82] The hydrogel exhibits up to 2400% tensile strain and excellent reversible bonding properties. The presence of sulfonic acid groups also makes the hydrogels sensitive to deformation, and the wearable sensor designed according to this characteristic, worn on the sole, can monitor the movement in real-time during running (Fig. 2d). Furthermore, Zhang *et al.* fabricated NaCl/SA/PAM supramolecular ionic hydrogels using complex-shaped supramolecular sodium alginate (SA).[83] An extremely wide strain window (0.3–1800%) and high pressure sensitivity are achieved by using ionic conductors as wearable sensors. This NaCl/SA/PAM hydrogel can sense compressive stress due to geometry change (Fig. 2e). The NaCl/SA/PAM hydrogel-based sensor can monitor the subtle pressure difference of a human wrist pulse before and after exercise (Fig. 2f).

However, most hydrogels will suffer from dehydration in practical applications due to their poor water-holding capacity. In addition, at subzero temperatures, they inevitably become hard, brittle, and poorly conductive due to the freezing of water, which easily loses many of the advantages of hydrogels. These drawbacks greatly hinder the application of conductive hydrogel-based devices in a real application environment. Introducing specific salts or nonvolatile solvents into the ionic gels can effectively address some of the above issues. For example, ionic gels containing hygroscopic salts (*e.g.*, LiCl) or glycerol have enhanced water retention capacities.[84,85] Ionic gels containing $CaCl_2$ or cryoprotectant solutions (such as ethylene glycol (EG), glycerol, and sorbitol) do not freeze and retain high stretchability at temperatures far below 0 °C.[62,86] In this strategy, strong hydrogen bonds are reported to be formed between water molecules and anti-freezing solvents, which could hinder water evaporation under ambient conditions. Ionic liquid (IL)-based ionic conductors have received extensive attention due to their non-volatility and excellent thermal stability.[87,88] The frost resistance and temperature resistance can be significantly improved by adding ionic liquids to the polymers. Jiao *et al.* designed a double network (DN) hydrogel incorporating zwitterionic proline (ZP) into gellan gum/polyacrylamide (GG/PAM).[61] The Ca-GG/PAM-ZP DN hydrogel exhibits excellent freezing resistance and adhesion. The adhesion of the hydrogel can reduce the gap between the hydrogel and the matrix, thereby maximizing the transformation of deformation from human motion into electrical signals. Furthermore, the zwitterionic hydrogel-based strain sensor can accurately monitor human motion from −40 to 25 °C. Fig. 2g shows the steady change of $\Delta R/R_0$ during finger bending when worn on the prosthetic hand at −40 °C. When worn on the finger at 25 °C, the $\Delta R/R_0$ exhibits a step-like change with increasing bending angle (Fig. 2h). Ma *et al.* prepared a novel ionic hydrogel of PAM using 1-ethyl-3-methylimidazolium chloride ([EMIM]Cl) as an ionic liquid.[89] This strategy achieves high transparency and water retention properties, which are critical for visual access to information and external light stimulation. The multiple hydrogen bonds between [EMIM]Cl and the polymer chains of the hydrogel endow the ionic hydrogel with high mechanical properties and excellent long-term water retention properties, which can achieve no loss of mechanical and electrical properties for more than 30 days. Fig. 2i shows that the weight of the ionic hydrogel shifted slightly (less than 16%) after being exposed to 25 °C for one month, and still showed flexibility. Moreover, the ionic hydrogel simultaneously possesses excellent water retention properties, high electrical

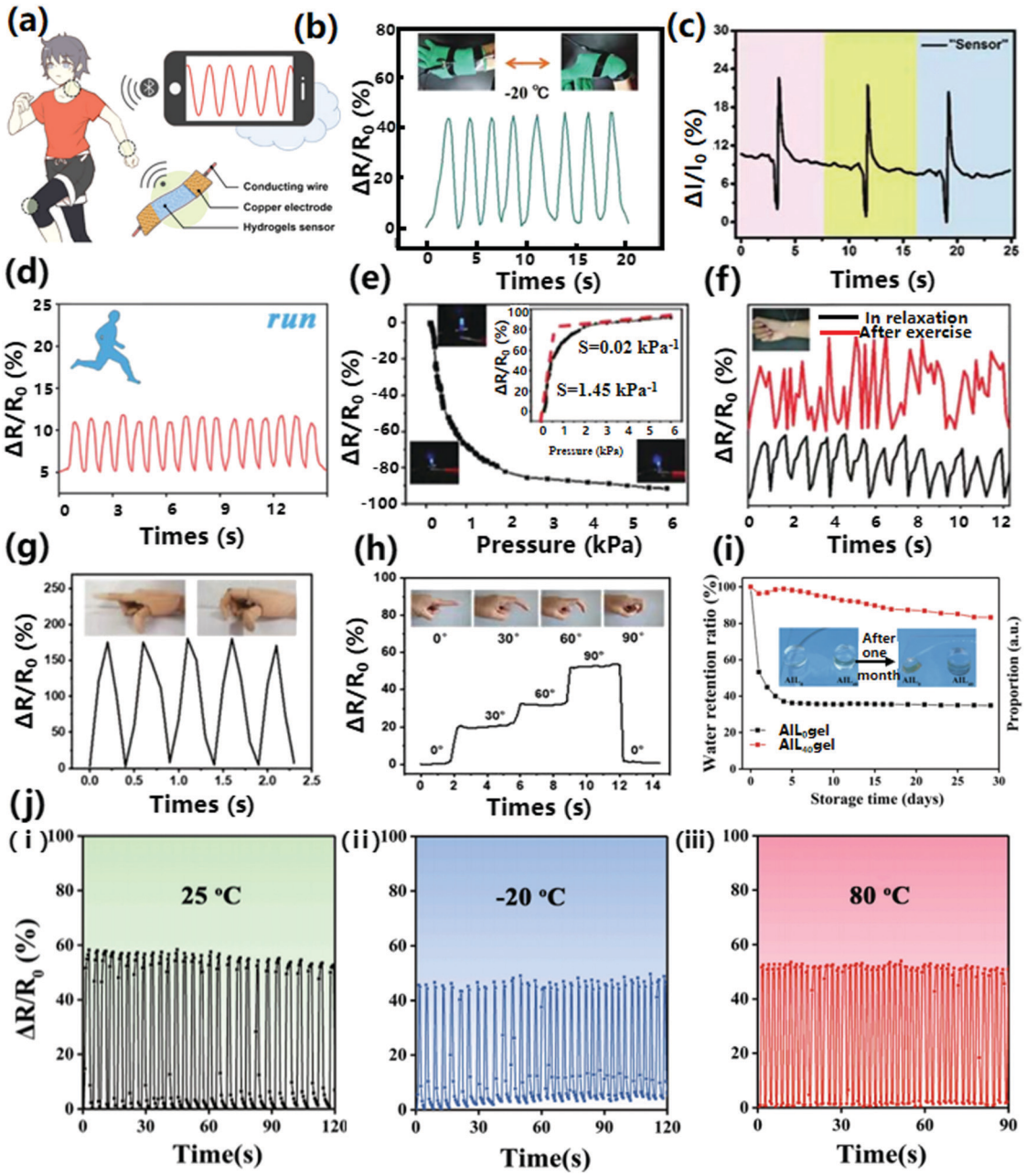

Fig. 2 (a) A PVA-PA hydrogel structure transmitted *via* bluetooth and a wearable display for a smartphone (reprinted with permission from ref. 75 Copyright 2019 American Chemical Society). (b) Real-time response of the PGN sensor to wrist flexion at −20 °C (reprinted with permission from ref. 76 Copyright 2020 Royal Society of Chemistry). (c) PAM/PVA hydrogel sensor detection "sensor" (reprinted with permission from ref. 77 Copyright 2018 Wiley). (d) The P(AM/AMPS)-AFPS hydrogel pressure sensor monitors the running process (reprinted with permission from ref. 82 Copyright 2020 Royal Society of Chemistry). (e) Relative resistance and sensitivity changes of the NaCl/SA/PAM hydrogel sensor during compression. (f) The NaCl/SA/PAM hydrogel sensor monitors the relative resistance changes of the pulse before and after exercise (reprinted with permission from ref. 83 Copyright 2019 Royal Society of Chemistry). Finger bending sensing test of (g) Zwitterionic Ca-GG/PAM-ZP hydrogel at −40 °C and (h) finger bending angle sensing test in a normal environment (reprinted with permission from ref. 61 Copyright 2021 American Chemical Society). (i) The water retention curve of the ionized hydrogel after one month of storage under natural conditions. (j) The process of the ionized hydrogel sensor stored at (i) 25 °C, (ii) −20 °C and (iii) 80 °C for 24 hours to detect the process of active robotic finger resistance response to signal (reprinted with permission from ref. 89 Copyright 2021 Elsevier).

conductivity, high transparency, frost resistance, heat resistance and long-term stability. The wearable sensor fabricated by an ionic hydrogel can realize human sensing in a wide temperature range (−20 °C to 80 °C) (Fig. 2j), showing excellent temperature resistance and stability.

2.1.3 PAA-based. Wang *et al.* prepared a Fe-sulfonated lignin (SL)-*g*- polyacrylic acid (PAA) hydrogel, which can be used for electronic coating products.[90] The combination of SL-metal ion (Fe^{3+}/Fe^{2+}) chelate and –COO– enables the Fe-SL-g-PAA hydrogel to self-heal. In Fig. 3a, both sides of the fracture

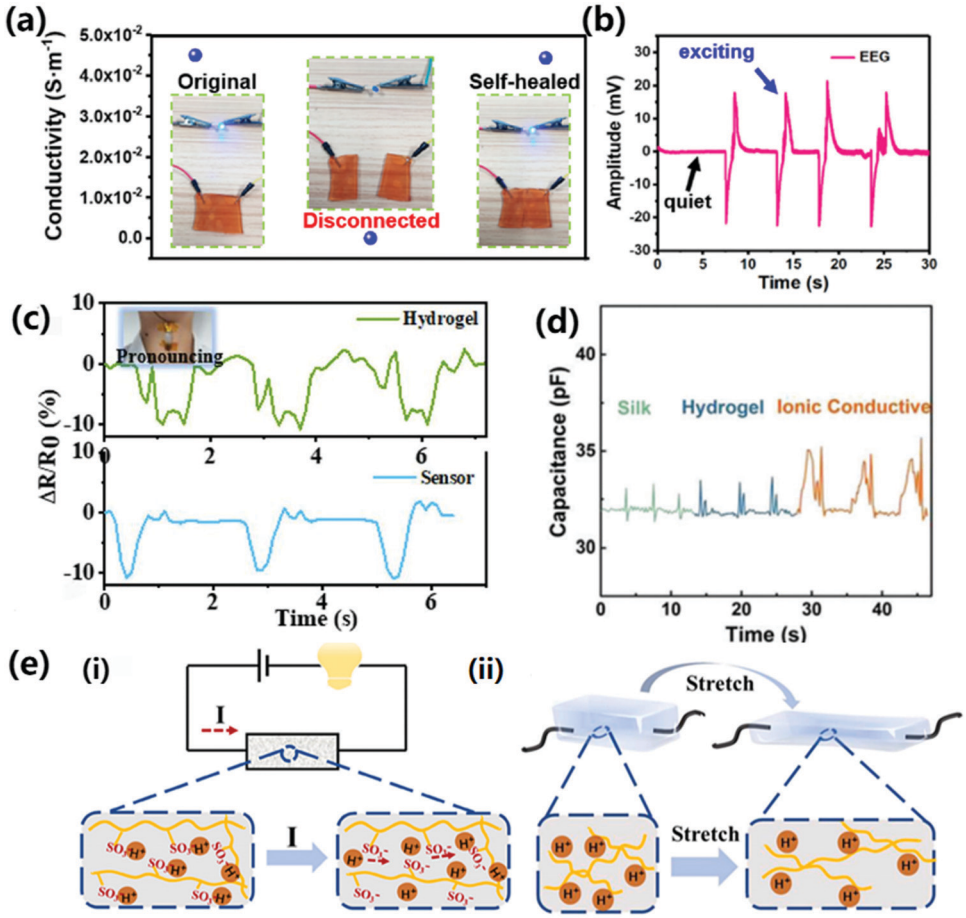

Fig. 3 (a) Photograph of a Fe-SL-g-PAA hydrogel repairing its electrical conductivity after cleavage. (b) EEG monitoring of a wearable bioelectronic device assembled from a hybrid of hydrogel coating and substrate (reprinted with permission from ref. 90 Copyright 2020 Royal Society of Chemistry). (c) The resistance response curves of a CNC/PAA hydrogel-based strain sensor monitoring someone reading "sensor" and "hydrogel" (reprinted with permission from ref. 91 Copyright 2021 American Chemical Society). (d) Movement patterns of the throat when different words were recorded from the RSF/$CaCl_2$/HRP hydrogel (reprinted with permission from ref. 62 Copyright 2021 Royal Society of Chemistry). (e) (i) The conduction mechanism of the PAMPS hydrogel. (ii) Schematic illustration of the resistance change during stretching (reprinted with permission from ref. 63 Copyright 2021 Elsevier).

in Fe-SL-g-PAA can complete 98.5% repair effect in 12 h and maintain conductivity. Based on these results, a strain sensor was fabricated using a Fe-SL-g PAA hydrogel, which could stably receive strain signals. Electroencephalography (EEG) was carried out with the hydrogel coating in both resting and excited states (Fig. 3b). Ma *et al.* utilized cellulose nanocrystals (CNCs) combined with PAA-based conductive hydrogels to achieve tensile strain and pressure-sensing capabilities.[91] This CNCs/PAA hydrogel has super stretchability and electrical conductivity and rapid self-healing. Transparent wearable sensors based on CNCs/PAA can sense various human motions. Fig. 3c shows the resistance response curve of the human throat when the words "sensor" and "hydrogel" are read out with the CNCs/PAA hydrogel sensor. It is worth noting that the unique sound monitoring waveform makes the sensor have certain potential in wearable voice assistants.

2.1.4 Other substrates. Zhao *et al.* prepared RSF/$CaCl_2$/HRP hydrogels by cross-linking regenerated silk fibroin (RSF) and contained horseradish peroxidase (HRP).[62] The obtained RSF/$CaCl_2$/HRP hydrogel exhibits high stretchability and transparency as well as self-adhesion. More importantly, the RSF/$CaCl_2$/HRP hydrogel possesses both strain and temperature sensing capabilities. Therefore, it can be assembled into a dual strain/temperature sensor. When tested as a wearable strain sensor, it was possible to record patterns of throat movement with different words, such as "silk," "hydrogel," and "ionic conduction." (Fig. 3c). Mao *et al.* fabricated a hydrogel sensor using 2-acrylamido-2-methylpropanesulfonic acid (AMPS) and *N,N'*-methylenebisacrylamide (MBA).[63] PAMPS hydrogels can conduct electricity due to the presence of ionizable sulfonic acid groups. The hydrophilic sulfonic acid is ionized, and the ions move directionally under the action of an external electric field, as shown in Fig. 3e(i). As shown in Fig. 3e(ii), when stretched, the polymer chains of the hydrogel are elongated and the change in ionic spacing leads to an increase in resistance. The hydrogel exhibits excellent transparency and strain sensitivity, which can be used for sensitive electrical conductivity monitoring of body motion and applied to wearable devices without obstructing optical markers.

2.2 Applications of human–computer interaction

In recent years, the development of artificial intelligence and attending gradual maturity in cutting-edge technology leads to flexible and wearable sensors, as a bridge between human's vision and forefront machine, have intrigued many researchers for their gripping features, such as high flexibility, sensitivity, portability, practicality and low cost. Owing to these advantages, they possess promising applications in wearable electronic devices for human motion detection, healthcare monitors, and medical diagnosis – only *via* contact with human skin or clothing. Inspired by human monitoring, wearable hydrogel sensors are gradually being developed in human–computer interaction devices. Worn on the body, the device can accurately monitor the signals emitted by the human body and convert them into digital signals or instructions to achieve more complex human monitoring. In addition, the use of transparent hydrogels is more in line with the future trends of beautiful, concealed, and lightweight human-machine interfaces.

2.2.1 PAM-based. Transparent hydrogel sensors have shown excellent performance in human health monitoring due to their stretchability, transparency and biocompatibility. The hydrogel worn on the surface of human skin produces macroscopic deformation through the process of human movement, which is accompanied by the movement of internal ions on the microscopic level and emits different electrochemical signals. Inspired by human monitoring sensing, Wu *et al.* synthesized a hydrogel using PAM and 2-aminoethylacrylamide hydrochloride (AEAM) as raw materials.[92] The hydrogel is combined with an eye mask and worn on the body to monitor the quality of human sleep. Fig. 4a simulates the sensing principle of this smart eye mask. The relative resistance change frequency caused by the eyeball rotation can clearly identify the situation of the sleep process. Compared with common sleep monitoring mobile applications, the recognition of REM sleep by the sleep process measured using the smart sleep mask showed higher reliability. The total REM time was calculated as 1 h 55 min. Compared to the average REM sleep time (25%) and polysomnography (PSG) commonly used in hospitals to monitor sleep, this sleep mask is less expensive and easier to use. It does not interfere with sleep, so it is more suitable for the general public.

Furthermore, Gu *et al.* fabricated a transparent wearable soft ionic electronic skin (iSkin) system using lithium chloride (LiCl) and polyacrylamide (PAM).[93] The iSkin system is combined with sign language, and when the fingers are bent/straightened, both are captured and wirelessly transmitted from the iSkin system to the virtual device (such as mobile phone). The remote virtual device can then translate the information into text. This work depicts the simulation process of different combinations of gestures representing "HELLO SJTUER". Lee *et al.* prepared a PAM/lithium chloride (LiCl)/trichlorosilane (HDFS) hydrogel.[94] Under the premise of ensuring high transparency and stretchability, a thimble-type wireless real-time communicator for the human-machine interface is designed based on static integrated circuits (HMI). The hydrogel is attached to the finger and coded using a single-chip microcomputer as 2^0-thumb, 2^1-index finger, 2^2-middle finger, 2^3-ring finger, and 2^4-little finger. Text can be expressed to wireless electronic devices through the combination of finger touch and a thimble-type static sensor, and the combination of finger signals is interpreted as

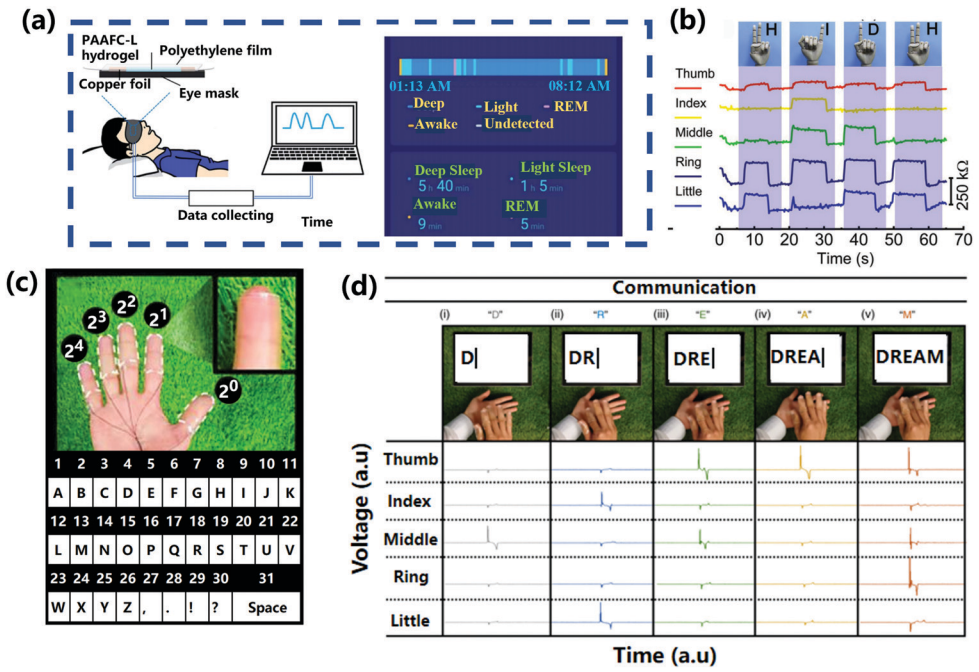

Fig. 4 (a) Device diagram of "Sleep Monitor" and sleep records obtained in the mobile phone program (reprinted with permission from ref. 92 Copyright 2020 Royal Society of Chemistry). (b) Organohydrogel fibers respond to the gestures for the letters H, I, D, and H in International Sign Language in real-time (reprinted with permission from ref. 72 Copyright 2020 Wiley). (c) Communication coding principle of the wireless communicator (STAIC). (d) STAIC expresses the "DREAM" signal through a combination of finger touches (reprinted with permission from ref. 94 Copyright 2018 Springer Nature).

Table 1 Performance of various hydrogels for preparing wearable strain sensors

Materials	Transmittance (%)	Strain (%)	Stress (KPa)	Self-healing	Conductivity (S m^{-1})	Adhesion	Ref.
PVA/PA	>95%	1100	—	Yes	0.13	Yes	75
PVA/glycerin/NaCl	>88%	570.7	3100	No	Conductive	No	76
PVA/PAM	>90%	>500	≈200	No	Conductive	Yes	77
AFPS/**PAM**/AMPS	>90%	≈1500	≈50	No	Conductive	Yes	82
NaCl/SA/**PAM**	99.6%	3120	750	Yes	0.01	No	83
Ca-GG/**PAM**/ZP	98.1%	1890	410	No	0.215	Yes	61
([EMIM]Cl)/**PAM**	94.36%	1160	≈25	No	3.886	No	89
Fe-SL-g-**PAA**	99.7%	1680	60	Yes	0.07	Yes	90
CNC/**PAA**	> 90%	2000	190	Yes	Conductive	Yes	91
RSF/$CaCl_2$/HRP	85%	600	20	Yes	0.17	Yes	62
PAMPS	93%	509.48	91.7	Yes	Conductive	Yes	63
PAM/AEAM/MWCNT	Transparent	1200	147	Yes	3.96	Yes	92
PAM/LiCl	95%	300	—	No	Conductive	No	93
PAM/LiCl/HDFS	99.6%	330	—	No	Conductive	No	94
PEG/$CaCl_2$/KCl	Transparent	≈400	≈200	No	0.765	No	72

shown in the alphabet (Fig. 4c). Fig. 4c demonstrates the principle of the wireless real-time communicator sending out a "DREAM" signal. When the letter "D" is entered, the number 4 in the alphabet (Fig. 4c) is represented by a single middle finger (Fig. 4d(i)). The numerical value of "*R*" is 18, which requires the thumb and little finger to be synchronized (Fig. 4d(ii)). Writing "E", "A", and "M" is based on the same mechanism.

2.2.2 Other substrates. Song *et al.* established a process for spinning hydrogel fibers of alginate and polyethylene glycol diacrylate hydrogel fibers, resulting in organohydrogel fibers that can operate at −80 °C and are stable in the long-term in an environment store.[72] They fabricated a strain sensor based on a wrist strap woven using organic hydrogel fibers and ordinary fabrics for detecting strain in different directions. The smart electronic data glove based on this transparent hydrogel can effectively recognize the hand gestures of the letters H, I, and D in the International Sign Language in sequence and recognize the words "HI, DH" (Fig. 4b). The system provides a great idea for blind typing or converting language into machine-readable and outputting sounds.

2.3 Brief conclusion

Wearable strain sensors have been widely used in human health monitoring, intelligent robots, electronic skin, human–computer interaction, wearable devices and other fields. Wearable strain sensors monitor human activity by converting their own deformations into electrical signals. In recent years, more and more flexible wearable sensors have been developed, which have high strength, excellent electrical conductivity, strong adhesion, and accurate detection of human health. Its applicability will be expanded by integrating various functions, including electrical conductivity, adhesion, self-healing, *etc.*, into hydrogel-based wearable strain sensors (Table 1).

3. Transparent stretchable pressure sensors

Hydrogel pressure sensors convert pressure into detectable or readable signals, such as resistance, capacitance, voltage, *etc.* This is based on the piezoresistive effect of hydrogels in the process of elastic deformation, which has the advantages of good signal acquisition performance, simple structure, and easy manufacturing. In recent years, hydrogel pressure sensors have also been widely applied in intelligent systems, such as timely health monitoring, precision surgery, artificial skin, wearable devices and soft robots. Because the transparent hydrogel pressure sensor has better optical diversity and wide adaptability, it can also be used in some smart interfaces such as touch screens and protective films. Here we present several transparent hydrogel pressure sensor applications categorized by material.

3.1 Independent object monitoring

The transparent hydrogel pressure sensor stably detects single objects. Due to the different forces of the monitored objects, high demands are placed on the pressure sensitivity of the hydrogel. In order to withstand large deformation, such transparent pressure sensors are usually made of elastic polymer materials, such as polyvinyl alcohol, polyacrylamide and other flexible materials.

3.1.1 PVA-based. A high-sensitivity and stretchable pressure sensor is prepared using a transparent hydrogel for human monitoring, which can sensitively monitor tiny external forces such as a pulse, throat, and heart. Inspired by human monitoring, Jing *et al.* developed a PVA/nanofiber (CNF) double-crosslinked hydrogel.[64] It is highly stretchable, transparent and biocompatible. Fig. 5a shows the principle of a pressure sensor based on this hydrogel design. The sensor consists of two hydrogel layers as electrodes with a layer of dielectric material sandwiched between them. When the hydrogel sensor is connected to an external power supply and capacitance meter, the ions (Na^+, Ca^{2+}, and Cl^-) inside the hydrogel are redistributed due to the electrostatic potential provided by the external power supply. Next, it was tested that the capacitance signal of the continuous falling water droplets on the sensor surface can be stably presented through capacitance changes (Fig. 5b).

3.1.2 PAM-based. Wang *et al.* successfully fabricated a multimode pressure sensor using zwitterionic gels and polyacrylamide-*n*-(2-hydroxyethyl)acrylamide (P(AM-*co*-HEMAA)) hydrogels.[68]

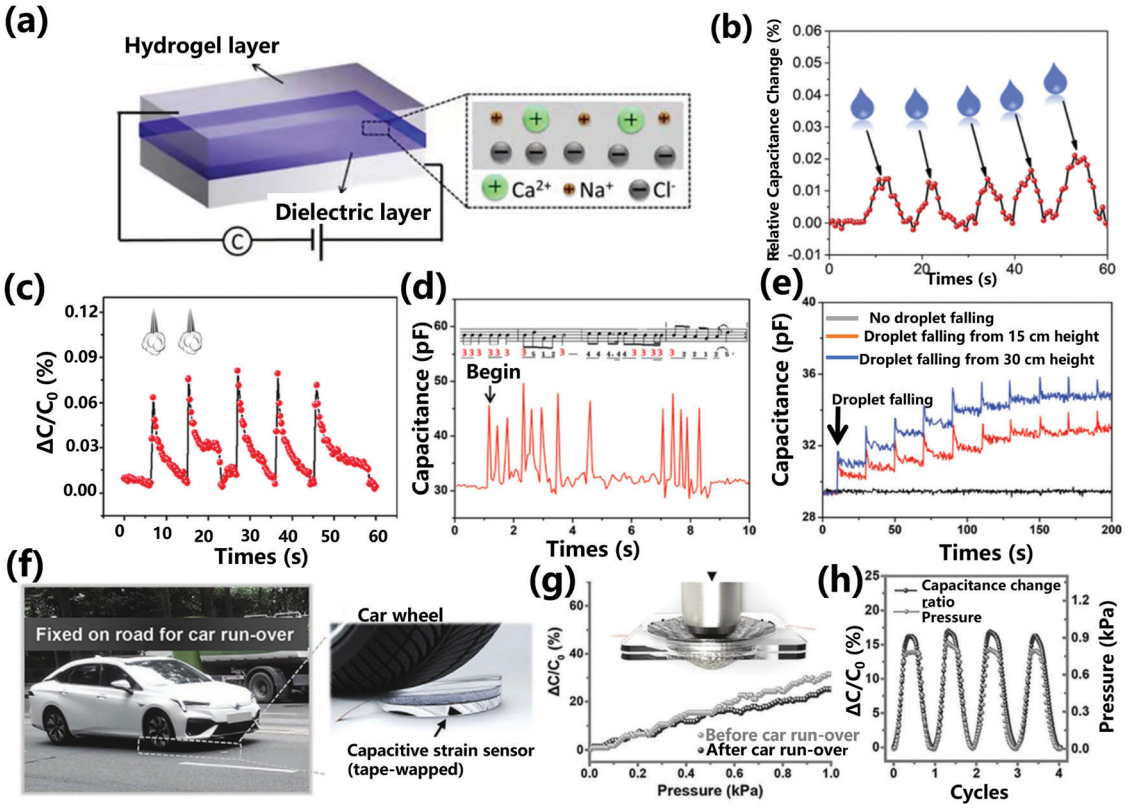

Fig. 5 (a) Structural diagram of the PVA/CNF hydrogel sensor. (b) The PVA/CNF hydrogel sensor monitors the relative resistance changes of falling water droplets (reprinted with permission from ref. 64 Copyright 2019 Elsevier). (c) Capacitive response curve of the AA/DMC hydrogel sensor monitoring weak dynamic airflow (reprinted with permission from ref. 68 Copyright 2020 Royal Society of Chemistry). (d) Real-time capacitance measurements of the ionic skin sensor in response to musical rhythms. (e) Real-time capacitive measurements of the ionic skin sensor response to water droplets falling continuously from different heights (reprinted with permission from ref. 95 Copyright 2019 Wiley). (f) Test plot of the zinc alginate/PAM hydrogel pressure sensor under extreme pressure conditions. (g) Capacitance curve of the zinc alginate/PAM hydrogel sensor before and after the car rolls. (h) The capacitance-pressure curve of the sensor in the automotive cyclic compression test (reprinted with permission from ref. 96 Copyright 2021 Wiley).

The pressure sensor based on this design can also be sensitive to the subtle dynamic airflow (0.7 N) (Fig. 5c). This can be explained by the fact that the kinetic energy of the air flow generates pressure immediately after reaching the sensor surface, most of which is converted into the strain energy of the hydrogel, resulting in the maximum capacitive output.

Yin *et al.* developed a dual-material hydrogel for ions for wearable and high-sensitivity ion-skin sensors.[95] The sensor is mounted on the "Mi" key of the phone's piano, and the capacitance changes rhythmically when the music is played (Fig. 5d). In addition, the fully-printed sensor can also monitor water droplets dropped from different heights (15 and 30 cm) onto the sensor surface and record the process of water droplets falling onto the sensor through the capacitance change of the sensor (Fig. 5e). Based on the realization of human body monitoring and water droplet monitoring, Mo *et al.* established a pressure sensor by integrating the dielectric layers of two ultra-tough organogels.[96] As shown in Fig. 5f, a car passes through the digital display scale equipped with the circular pressure sensor at a constant speed. The pressure detector gauge shows that the front and rear wheels exert 440 and 650 kg of force on the capacitive strain sensors, respectively. After being run over by 20 random vehicles, the capacitance-pressure curve of the pressure sensor showed no significant signal decay compared to the initial performance (Fig. 5g). In addition, as shown in Fig. 5h, the pressure sensor still works well under the repeated action of the frequency of 0.5 Hz. The assembled capacitive strain sensor is capable of withstanding the extreme compressive strength of a car roll.

3.2 Pressure sensor array

The development of bendable, stretchable, and transparent touch sensors is an emerging technological goal in various fields, including electronic skin, wearable devices, and flexible handheld devices. The transparent hydrogel-based pressure sensor demonstrated a good sensing effect after being subjected to an external force. Researchers combined multiple hydrogel sensors into sensor arrays to achieve multi-functional and complex applications.

3.2.1 PAM-based. A multi-mode pressure sensor was fabricated by Wang *et al.*[68] Sensors of the same volume are formed into a 4 × 4 sensor array model and numbered sequentially (Fig. 6a). To examine the spatial resolution performance of the sensor array, a 10 g steel ball was placed at C2. As shown in

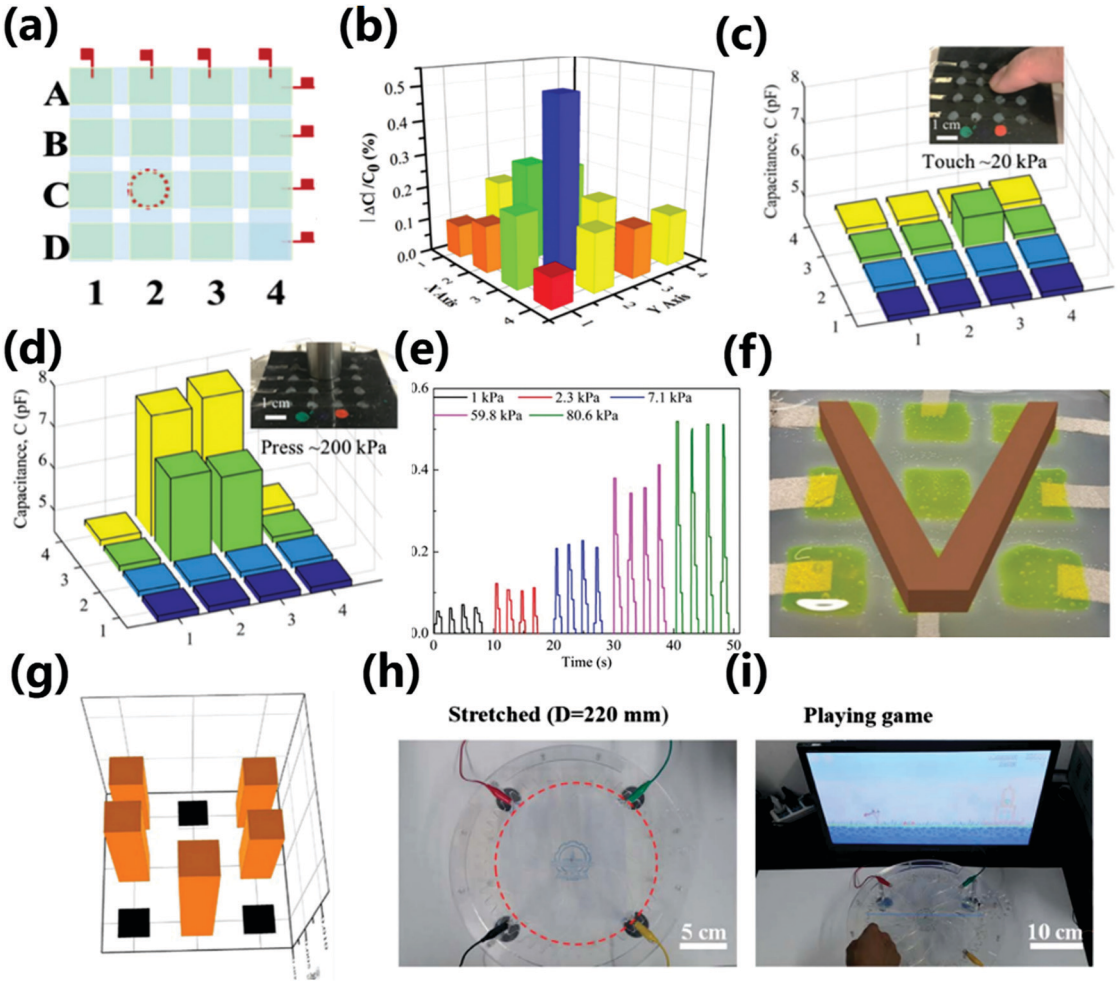

Fig. 6 (a) AA/DMC hydrogel sensor array cell model with steel balls placed in C2. (b) Spatial distribution model of sensor output (reprinted with permission from ref. 68 Copyright 2020 Royal Society of Chemistry). (c) 4 × 4 arrays of finger touch and (d) multi-node pressure sensing (reprinted with permission from ref. 69 Copyright 2019 Wiley). (e) Representative voltage generation performance of compressed EWL-TNEG as a pressure sensor. (f) Photograph and (g) the corresponding voltage generation of the EWL-TENG sensor array (3 × 3 patch pattern) with V-shaped loading under repeated approach-separation motions (reprinted with permission from ref. 70 Copyright 2020 Wiley). (h) PDMAA/TiO_2-based circular touch panel stretched to a diameter of 220 mm. (i) The touch panel still works when stretched (reprinted with permission from ref. 99 Copyright 2021 Royal Society of Chemistry).

Fig. 6b, due to the deformation in the entire plane caused by the weight of the steel ball, a three-dimensional capacitance change distribution is generated. It can be seen that the maximum change and the change of adjacent units are consistent with the position of the loading pressure, which accurately reflects the specific spatial distribution. Charaya *et al.* fabricated a 4 × 4 bimodal sensor array for multiplex sensing.[69] In the non-pressed state, the initial capacitance measurements for all sensors were 4.65 ± 0.04 pF. As shown in Fig. 6c, when a finger gently touches any node, the capacitance of the corresponding position sensor increases, while the capacitance of other nodes remains unchanged. Fig. 6d shows that the corresponding node capacitance will change to demonstrate multi-node sensing by pressing multiple nodes simultaneously.

3.2.2 Other substrates. A transparent egg white hydrogel was cleverly prepared by Chang *et al.*[70] The transparent hydrogel exhibits good self-healing properties and an ionic conductivity of 20.4 S m^{-1}. As shown in Fig. 6e, the limitation of pressure detection was around 1 KPa with the voltage being reached to 0.05 V, and the voltage increased to about 0.52 V when elevating the external pressure to 80.6 KPa. Meanwhile, the generated voltage profile kept a similar amplitude and shape in the same pressure cycles. A highly compressible and transparent nanotriboelectric generator (TENG) was fabricated using hydrogels. Then another sensing array was fabricated by exploiting the pressure-sensitive properties of TENG. 3 × 3 hydrogel patches were printed on the Ecoflex film, and when a V-plate was placed on the array, each patch sensed the pressure on it and generated a voltage independently (Fig. 6f and g).

3.3 Intelligent electronic touch panel

With the development of science and technology, human–computer interaction is becoming more and more important. Through the sensitive detection effect and excellent sensing

Table 2 Performance of various hydrogels for preparing pressure sensors

Materials	Transmittance (%)	Strain (%)	Stress (KPa)	Self-healing	Conductivity (S m^{-1})	Adhesion	Ref.
PVA/CNF	>90%	1900	11.2	Yes	Conductive	No	64
PAA/DMC + PAM/HEMAA	>70%	300	100	Yes	0.2	Yes	68
PAM/PEGDA/Mg^{2+}	Transparent	630	158	No	Conductive	Yes	95
Zn-Alginate/PAM	Transparent	>600	2100	No	3.24	Yes	96
PAM/TLC	Transparent	Stretchable	200	No	Conductive	No	69
Protein solution/ecoflex	99.8%	100	80	No	20.4	Yes	70
PAM/LiCl	98%	1000	12	No	Conductive	No	97
PDMAA/TiO_2	Transparent	1100	30	Yes	Conductive	No	99

performance of transparent hydrogel pressure sensors, more and more researchers have seen that transparent pressure sensors can detect external pressure stimuli and present them through electrical signal changes. Moreover, these hydrogels have both scalability and reversible recovery, and these advantages can be better applied in the field of soft electronic devices such as smart touch templates. Among the various types of touch-sensing systems, the same voltage is applied to all corners of the touch panel, which results in a uniform electrostatic field across the panel. When a conductor, such as a human finger, touches the panel, the touchpoint becomes grounded, generating a potential difference between the electrode and the touchpoint. The potential difference causes the current to flow from the electrode through the finger. The magnitude of the current is determined by the distance between the touch point and electrode. As the distance decreases, a larger current is induced. By measuring the change of the current by two ammeters, the position of the touch point can be determined.

3.3.1 PAM-based. For example, Kim *et al.* demonstrated an ionic touchpad based on a polyacrylamide hydrogel containing lithium chloride salts.[97] Since the hydrogel is transparent, the panel can transmit light information freely, with a transmittance of 98% to visible light. This work introduces the design principle of 2D touch screens, the panel is connected to the computer through the control panel, and the computer displays the output numbers on the No. 2 display according to the signal of the control panel. When a human figure is drawn on the ion touchpad, it can be seen that the corresponding human figure appears on the same calculator.

3.3.2 Other substrates. Sarwar *et al.* fabricated a touch sensor based on a polyurethane hydrogel.[98] The sensor consists of polyurethane hydrogels swollen with different salt solutions. The electrical signal response of the hydrogel is derived from the voltage and current signals generated by the internal ion differential. Finger clicks on conventional touchscreen devices were simulated using polyurethane hydrogels, proving the potential of polyurethane hydrogels as touchpads, *etc.* Guo *et al.* fabricated a touchpad based on poly(*N*,*N*′-dimethylacrylamide)-titania nanocomposite hydrogels.[99] Due to the excellent stretchability, biocompatibility and self-healing properties of hydrogels, it can play an important role in touch-sensitive panels. A circular touchpad (diameter = 65 mm) is fixed on the console and connected to the computer. When the touchpad was pulled even to a diameter of 220 mm, the touchpad area increased by 1100% (Fig. 6h). Furthermore, the touchpad remains functional as a touch element at such high stretches (Fig. 6i).

3.4 Brief conclusion

The transparent hydrogel group shows good potential as an ionic conductor due to its flexibility and natural biocompatibility. The pressure sensor based on this design has excellent anti-compression, sensitive effect, and has an excellent performance in soft electronic devices (Table 2).

4. Transparent stretchable temperature sensors

Temperature sensing is an essential activity in our daily life. Traditional temperature sensors are prepared by spraying or depositing sensing materials on flexible substrates. However, most of these sensors are made on flat substrates with low transparency, low stretchability, a limited detection range, *etc.*[67] Compared with the traditional temperature sensor, a transparent stretchable hydrogel sensor is more suitable for real-time monitoring of human body temperature with ionic skin and can visualize the human-machine interface. We divide transparent stretchable temperature sensors into two categories: single response (electrical resistance change) and dual response (both resistance and transparency change) transparent stretchable temperature sensors.

4.1 Single response transparent stretchable temperature sensor

The single response transparent stretchable temperature sensor is the electrical resistance of the hydrogel sensor based on ionic conductivity changes with the temperature. The principle of the temperature sensor is shown in Fig. 7a. Ion migration is a thermally activated process, as the temperature increases, the mobility of ions increases. In addition, the increase of temperature promotes the decomposition of ions and increases the concentration of carriers.[100] Therefore, with the rise of temperature, the conductivity of the hydrogel is positively shifted and its resistance decreases rapidly. The single response transparent stretchable temperature sensor can provide real-time temperature feedback and has the advantages of visual beauty and visualization. Below, we introduce transparent stretchable temperature sensors based on transparent hydrogel substrates, including polyacrylamide (PAM), polyvinyl alcohol (PVA), *etc.*

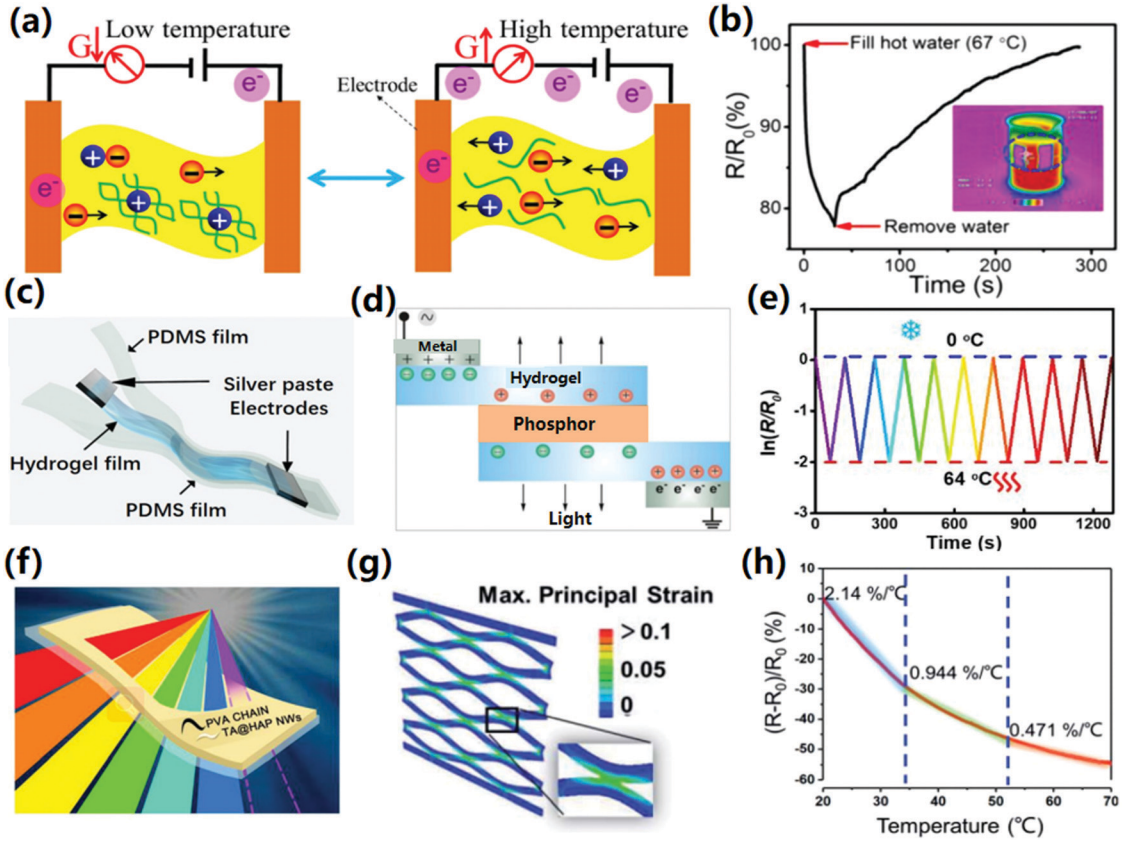

Fig. 7 (a) Schematic illustrating the temperature sensing principle of the organic hydrogel (reprinted with permission from ref. 100 Copyright 2020 American Chemical Society). (b) Dynamic response curves of the hydrogels fill hot water (67 °C) and remove water. The illustration is an infrared image of a thermosensitive hydrogel placed on a beaker filled with hot water (reprinted with permission from ref. 101 Copyright 2018 American Chemical Society). (c) Schematic diagram of a hydrogel film encapsulated and assembled into a sandwich structure (reprinted with permission from ref. 65 Copyright 2021 American Chemical Society). (d) Diagram of a luminescent device in which the phosphor layer is sandwiched between two transparent hydrogel layers and emits light when an AC voltage is applied (reprinted with permission from ref. 66 Copyright 2019 American Chemical Society). (e) The hydrogel temperature sensor's relative resistance's real-time response was cycled ten times in the thermo-cooling cycle of 0–64 °C (reprinted with permission from ref. 102 Copyright 2020 Royal Society of Chemistry). (f) Mechanism diagram of TA@HAP NWs reflecting ultraviolet light and transmitting visible light (reprinted with permission from ref. 103 Copyright 2021 Wiley). (g) The strain distribution of the customized kirigami strain-sensitive components. (h) Real-time response and temperature sensitivity diagram of the relative resistance of temperature sensor with temperature change (reprinted with permission from ref. 71 Copyright 2020 Royal Society of Chemistry).

4.1.1 PAM-based. It is found that the PAM/carrageenan (CA) double network (DN) hydrogel is highly sensitive to temperature and therefore can be exploited as a novel channel material for a thermistor. Wu *et al.* developed a thermistor for the first time using a PAM/CA DN hydrogel with ultra-high tensile, good transparency and self-healing ability.[101] For practical temperature sensing, the thermistor can be mounted on non-flat surfaces, such as curved glass surfaces. When hot water (67 °C) is poured into the cup, the device's resistance is immediately reduced. After removing the hot water, the resistance value is restored to the initial value (Fig. 7b). The self-healing behavior of the hydrogel is mainly due to the following two aspects. On the one hand, the thermos-reversible sol–gel transition and the coil-helix structural transition of CA in aqueous media above its sol–gel transition temperature can repair the furcated surfaces. On the other hand, the hydrogen bond interaction between PAM and CA can automatically repair the soft hydrogel at the broken interfaces. Wu *et al.* found that solvents play a key role in the thermal sensitivity of hydrogels for the first time.[100] So they fabricated ethylene glycol (Eg)/glycerol (Gly)/PAM/CA organic hydrogels by introducing Eg/Gly, which partially replaced water in hydrogels. Thanks to the ionic transport property and water-Eg/Gly binary solvent, the organohydrogel achieves an unprecedented thermal sensitivity of 19.6%/°C, and the hydrogel was endowed with anti-drying and anti-freezing properties. Wu *et al.* designed a novel thin-film sandwich structure (TFSS) stretchable and transparent temperature sensor based on PAM/CA.[65] As shown in Fig. 7c, by wrapping the thin hydrogel layer (12.15 μm) with two thin elastomer layers (polydimethylsiloxane (PDMS)), the water evaporation of the hydrogel is prevented, the heat transfer ability is enhanced, the stability is improved, and the response/recovery speed is accelerated. The TFSS temperature sensors displayed an unprecedented temperature sensitivity (24.54%/°C), rapid response time (0.19 s) and recovery time (0.08 s), high resolution,

high transparency, and excellent stretchability. Furthermore, the digital picture of a bear behind the TFSS sensor can still be clearly seen at 30% tensile strain.

Yang *et al.* fabricated LiCl/agar/PAM ionic double-network hydrogels as temperature-strain sensors, which significantly improves the tensile capacity of the hydrogel, and the elongation exceeds 1600%.[66] The resistance continuously decreased as the temperature increased from ambient to 50 °C, which suggests the ionic hydrogel is a promising thermal sensor with a negative temperature effect. They assembled two transparent hydrogels with a dielectric layer sandwiched between them to produce flexible electroluminescent devices. As shown in Fig. 7d, this sandwich structure is equivalent to three shunt capacitors. The AC voltage causes an electric field generated by the ions of opposite polarity from the ionic hydrogel, lightening the intermediate emission layer. Typically, the transparent hydrogel scatters little light, allowing a variety of light colors from the middle emission layer to be transmitted.

4.1.2 PVA-based. Wang *et al.* used a quaternary ammonium hydroxide aqueous solution – benzyl trimethyl ammonium hydroxide ($BzMe_3NOH$) as a cellulose solvent to fabricate a highly stretchable, transparent ionic conductive cellulose/PVA hydrogel (CPH).[102] As shown in Fig. 7e, the temperature sensor based on CPH is cyclically monitored in a wide temperature range of 0–60 °C, showing a fast response time, high reliability and reversible resistance transition, indicating that the sensor has good thermoelectric reliability.

Transparent conductive hydrogels usually do not filter ultraviolet (UV) light. To solve this problem, Wen *et al.* added tannic acid-coated hydroxyapatite nanowires (TA@HAP NWs) with UV filtering capabilities to a hydrogel containing aluminum chloride, PVA, ethylene glycol (EG) and water (W), thus fabricating a TA@HAP NWs-PVA(EG/W) hydrogel.[103] The temperature sensitivity of the temperature sensor was calculated as 0.00536 $°C^{-1}$. The mechanism of TA@HAP NWs reflecting ultraviolet light and transmitting visible light is shown in Fig. 7f. TA@HAP NW_S has the same nanoscale diameter as short-wave ultraviolet light. Therefore, the short-wavelength ultraviolet light will be reflected (size effect) and absorbed multiple times by TA@HAP NWs. When natural light passes through the material, only a small amount of ultraviolet light remains, while visible light with a long-wavelength can pass through smoothly. The ability to absorb UV light waves of TA@HAP NWs may be related to the catechins in tannins acid.[104,105]

Inspired by the kirigami structure, Pan *et al.* fabricated cellulose nanofibrils (CNFs)/PVA/Gly/Ca^{2+} ion-conducting organohydrogel (ICOH).[71] Customized kirigami strain-sensitive components (Fig. 7g) enhance skin adaptability and sensing sensitivity. As shown in Fig. 7h, the temperature sensor based on ICOH exhibits a negative temperature coefficient behavior with the increase of temperature between 20–70 °C. And the temperature sensitivity decreased from 2.14%/°C to 0.471%/°C, which is attributed to the gradual increase in temperature, reducing the temperature difference between the temperature-sensitive component and the heat source, so it takes a longer time for the same temperature change value and the temperature sensitivity decreases.

4.1.3 Other substrates. Biocompatible hydrogels can be better used in healthcare and other fields. Wei *et al.* added 2-hydroxyethyl methacrylate (HEMA) and zwitterionic [2-(methacryloyloxy) ethyl] dimethyl-(3-sulfopropyl) ammonium hydroxide (SBMA) to sodium alginate to fabricate sodium alginate/HEMA/SBMA (AHS) hydrogel with no significant cytotoxicity.[106] An AHS hydrogel thin layer is used as a temperature sensor to simulate the human perception of temperature, and its temperature sensing mechanism is shown in Fig. 8a. When the artificial hand is close to the self-heating patch, the high temperature makes the hydrogel resistance decrease and the LED light becomes bright, realizing the temperature alarm function (Fig. 8b).

Hu *et al.* fabricated cellulose/sodium chloride (NaCl) hydrogel (CNH) by soaking chemically crosslinked cellulose in a sodium chloride aqueous solution to regenerate.[107] As shown in Fig. 8c, the temperature sensor assembled by CNH exhibits a temperature coefficient of resistance of -0.024 $°C^{-1}$. The capacitance of the pressure sensor based on the CNH hydrogel changes very little in the range of −15 to 50 °C, which can be ignored, indicating that it has good applicability as a pressure sensor in a wide temperature range (Fig. 8d). In addition, CNH-based hydrogels can be assembled into triboelectric nanogenerators (Fig. 8e). When a piece of latex touches the VHB layer and leaves, a layer of positive charge forms on the electrode and electrons flow through the electrode to the ground. When the latex comes into contact with the VHB layer again, the process is reversed. This contact-separation operation is cycled to produce an electric current.

When hydrogels respond to both temperature and pressure, interference and confusion of signals generated by different stimuli should be avoided. Chen *et al.* fabricated a regenerated silk fibroin (RSF)/silver nanowire (AgNWs)/calcium ion (Ca(II)) hydrogel and assembled it into a temperature/pressure sensing bimodal ionic skin.[108] As shown in Fig. 8f, the RSF/AgNW/Ca(II) hydrogel can recognize small temperature changes (such as 0.5 °C or 1.0 °C) and has high signal stability toward temperature changes. Put a warm serum bottle and a cold serum bottle on the hydrogel sensor array (Fig. 8g), and it can be clearly seen that the temperature sensing signal (Fig. 8h) and the pressure sensing signal are independent.

4.2 Dual-response transparent stretchable temperature sensor

In a dual-response transparent stretchable temperature sensor, when the temperature changes the electrical resistance of the hydrogel sensor changes, and the transparency changes from a transparent to an opaque state. The combination of temperature response and transmittance response enables the hydrogel sensor to have an adjustable visual effect at monitoring temperature and can be used for display and alarm. It has broad application prospects.

4.2.1 PEGDA-based. The polymer with the upper critical solution temperature (UCST)[109] was used as the hydrogel matrix to make the hydrogel undergo reversible phase

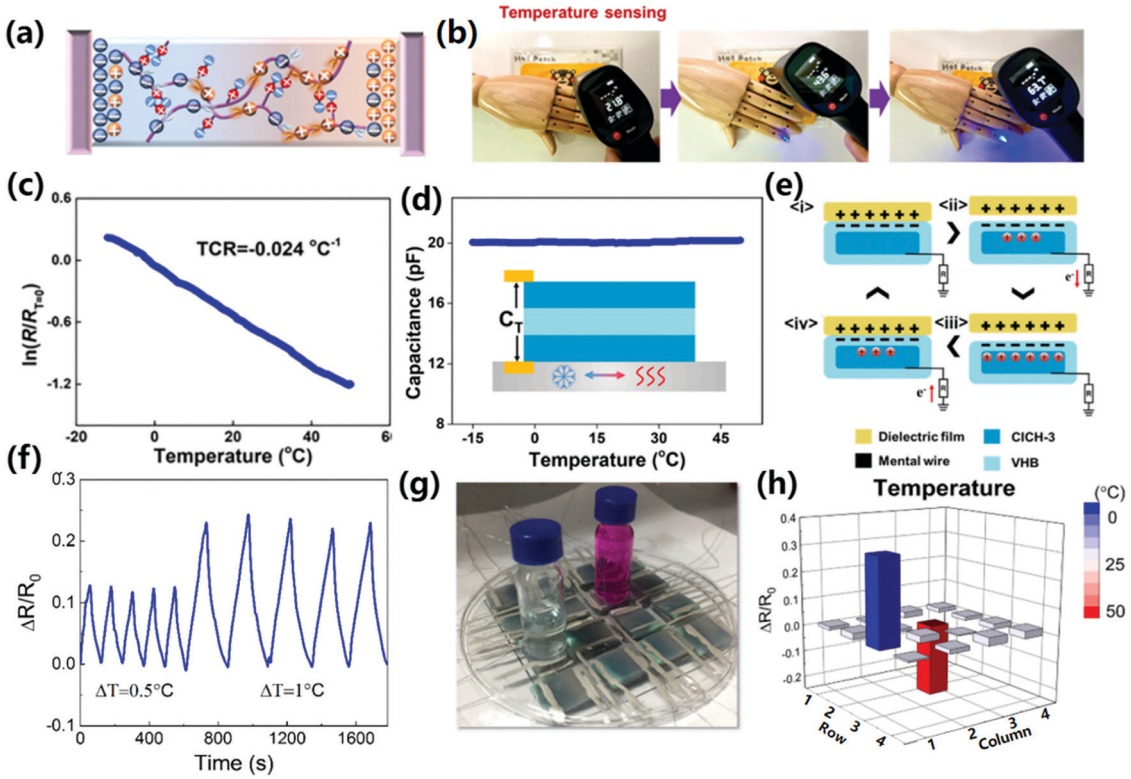

Fig. 8 (a) Schematic diagram of ion sensing and temperature sensing based on an AHS hydrogel. (b) Artificial hand close self-heating patch and temperature sensor alarm (reprinted with permission from ref. 106 Copyright 2021 American Chemical Society). (c) Real-time response of the relative resistance of the CNH-based temperature sensor to temperature change. (d) Capacitance response of the CNH-based pressure sensor with temperature. (e) Working principle diagram of a single electrode mode friction nanogenerator (reprinted with permission from ref. 107 Copyright 2021 Elsevier). (f) Real-time response of RSF/AgNW/Ca(II) hydrogel's relative resistance to small temperature changes. (g) Diagram of serum bottles containing water of different temperatures and weights placed on the RSF/AgNW/Ca(II) hydrogel array. (h) Temperature sensor monitoring of the sensor array in (g) (reprinted with permission from ref. 108 Copyright 2021 Elsevier).

transformation when the temperature was higher than or lower than the UCST. Therefore the transparency of the hydrogel sensor was changed at the same time as the temperature sensing. Inspired by mussels, Zhang *et al.* prepared dopamine-triggered gelation (DTG) sulfobetaine methacrylate (SBMA)/poly(ethylene glycol) diacrylate (PEGDA)/dopamine hydrogel by adding hydrochloride dopamine as a polymerization initiator and dynamic medium into the hydrogel.[110] As shown in Fig. 9a, the relative resistance of the DTG hydrogel decreases with the increase of temperature and shows a linear relationship, indicating that the hydrogel has excellent temperature-sensing sensitivity. The DTG hydrogel was used as a visual temperature sensor to monitor the changes in color and the temperature of the hydrogel (Fig. 9b). As shown in Fig. 9c, the hydrogel visual temperature sensor becomes opaque at 0 °C and transparent at 25 °C, and the process responds quickly and is reversible. The reason for the reversible color transformation is that PSBMA is a UCST polymer, and moderate dopamine content can prevent PSBMA from being highly crosslinked or inhibiting the intramolecular/intermolecular binding of PSBMA, resulting in UCST behavior.

4.2.2 PAA-based. Similarly, Shi *et al.* prepared a thermo-responsive QCS-polyacrylic acid (PAA) hydrogel (QAAH) with UCST from amphiphilic polymer quaternized chitosan (QCS) aqueous solution by *in situ* polymerizing acrylic acid (AA).[111] As shown in Fig. 9d, the transmittance of the hydrogel changes obviously in the thermal response phase transition process. When heated to the phase transition temperature, the hydrogel becomes transparent and opaque when cooled, and the volume change in this process can be ignored. The UCST of QAAH can be changed, which decreases with the increase of PAA content (Fig. 9e), and increases with the increase in pH value. As shown in Fig. 9f, the QAAH-based temperature sensor can accurately monitor body temperature.

4.2.3 TPU-based. Temperature sensors can also be prepared without any matrix polymers or additives. Choi *et al.* fabricated a time-temperature sensor by electrostatic spinning using thermoplastic polyurethane (TPU), a self-healing material.[112] As shown in Fig. 9g, electrospun nanofiber pads are opaque due to light reflection and scattering. Over time, the fibers aggregate to reduce thermodynamic free energy, resulting in less light scattering and a transparent, porous film. Half of the time-temperature indicator was placed in the dry icebox, and the other half was convection heated with a heat source of 80 °C. After 30 minutes, it could be seen that the part of the dry ice was still opaque, while the heated part became transparent (Fig. 9h).

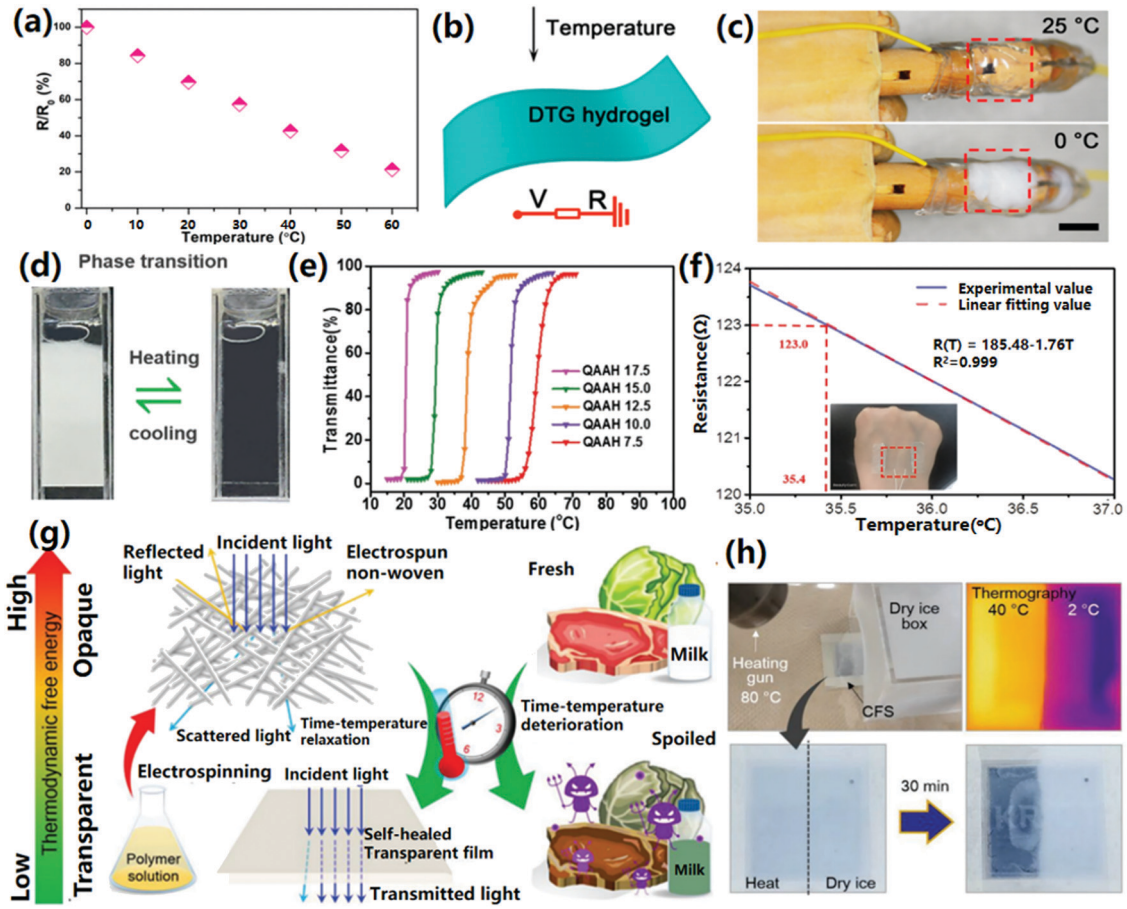

Fig. 9 (a) Real-time response of DTG hydrogel resistance to temperature change. (b) Schematic diagram of the visual temperature sensor prepared with a DTG hydrogel. (c) Diagram of the visualized temperature sensor at 25 °C and 0 °C (reprinted with permission from ref. 110 Copyright 2021 American Chemical Society). (d) Image of a reversible phase transition in QAAH as heated and cooled. (e) Relationship between light transmittance and temperature of QAAH with different AA content. (f) The QAAH-based temperature sensor monitors the electrical resistance as a function of body temperature (reprinted with permission from ref. 111 Copyright 2021 Wiley). (g) Time-temperature detector light transmittance changes with time and temperature, monitoring perishable food spoilage mechanism diagram. (h) The part of the time-temperature monitor senses the heat and changes the transmittance (reprinted with permission from ref. 112 Copyright 2020 Wiley).

Table 3 Performance of various hydrogels for preparing temperature sensors

Materials	Transmittance (%)	Strain (%)	Stress (KPa)	Sensitivity (%/°C)	Self-healing	Antifreeze	Ref.
PAM/CA/K^+	81%	330	—	2.6	Yes	No	101
Eg/Gly/**PAM**/CA/LiBr	Transparent	1103	36	19.6	Yes	Yes	100
PDMS sandwiched with **PAM**/CA	>90%	—	—	24.54	No	Yes	65
LiCl/agar/**PAM**	>90%	>1600	220	—	No	No	66
Cellulose/**PVA**	80.42%	747	37.3	−3	No	No	102
TA@HAP NWs-**PVA**(EG/W)	60%	480	360	0.536	No	Yes	103
CNFs/**PVA**/Gly/Ca^{2+}	93.8%	450	590	2.14(20–34 °C), 0.944(34–52 °C), 0.471(52–70 °C)	No	Yes	71
Alginate/HEMA/SBMA	96.2%	975	≈250	2.39	No	No	106
Cellulose/NaCl	94%	235	5200	−2.4	No	Yes	107
RSF/AgNWs/Ca(II)	Transparent	6	28	1.54(0–50 °C), 5.02 (−30 to 0 °C)	No	No	108
SBMA/PEGDA/dopamine	90% ↔ opaque	—	—	—	Yes	No	110
QCS/PAA	Transparent ↔ opaque	>2000	≈290	1.53	Yes	No	111
TPU	Opaque ↔ transparent	—	—	—	No	No	112

4.3 Brief conclusion

The temperature sensor increases the ion mobility by increasing the temperature so that the resistance of the sensor decreases (Table 3). Transparent stretchable temperature sensors can be used in wearable electronics, ionic skin, soft robotics and other fields.

5. Transparent stretchable humidity sensors

Humidity variation greatly affects the life and health of humans and electronic devices. Transparent stretchable humidity sensors are extremely suitable for monitoring respiration, healing conditions of wounds, skin hydration, metabolic status, *etc.* The humidity sensing mechanism is mainly ascribed to the swelling effect of hydrophilic groups on hydrogels/organo-hydrogels upon the absorption of water, so changing the electrical properties.[113] PAM, PVA, κ-CA, ethylene glycol (EG), glycerol (Gly), *etc.*, are common materials to fabricate transparent hydrogels, and they contain hydrophilic groups (–NH_2 or –OH or SO_3^-) on the polymer networks, which make the hydrogel have high humidity sensitivity. We divide the transparent stretchable humidity sensors into two categories: single response (electrical resistance change) and dual response (both resistance and color change) transparent stretchable temperature sensors.

5.1 Single response transparent stretchable humidity sensors

A single response transparent stretchable temperature sensor is the electrical resistance of the hydrogel sensor based on ionic conductivity changes with the temperature.[113] The transparent humidity sensor can be used in wearable masks and other devices to make them have better aesthetics. Below, we discuss such sensors according to different transparent substrate materials, then introduce the latest research.

5.1.1 PAM-based. Wu *et al.* reported EG/Gly modified k-CA/PAM double network (DN) organo-hydrogels humidity sensors.[113] In the process of changing from low relative humidity to high relative humidity, the concentration of the polymer chain decreases, which increases the ionic solubility of the polymer chain. As water is adsorbed and condensed on the organic hydrogel through physical and chemical adsorption processes, the blocking effect caused by the polymer chain decreases, so the resistance decreases and the sensing ability is enhanced (Fig. 10a). As shown in Fig. 10b, as the relative humidity (RH) in the chamber increases, the relative humidity

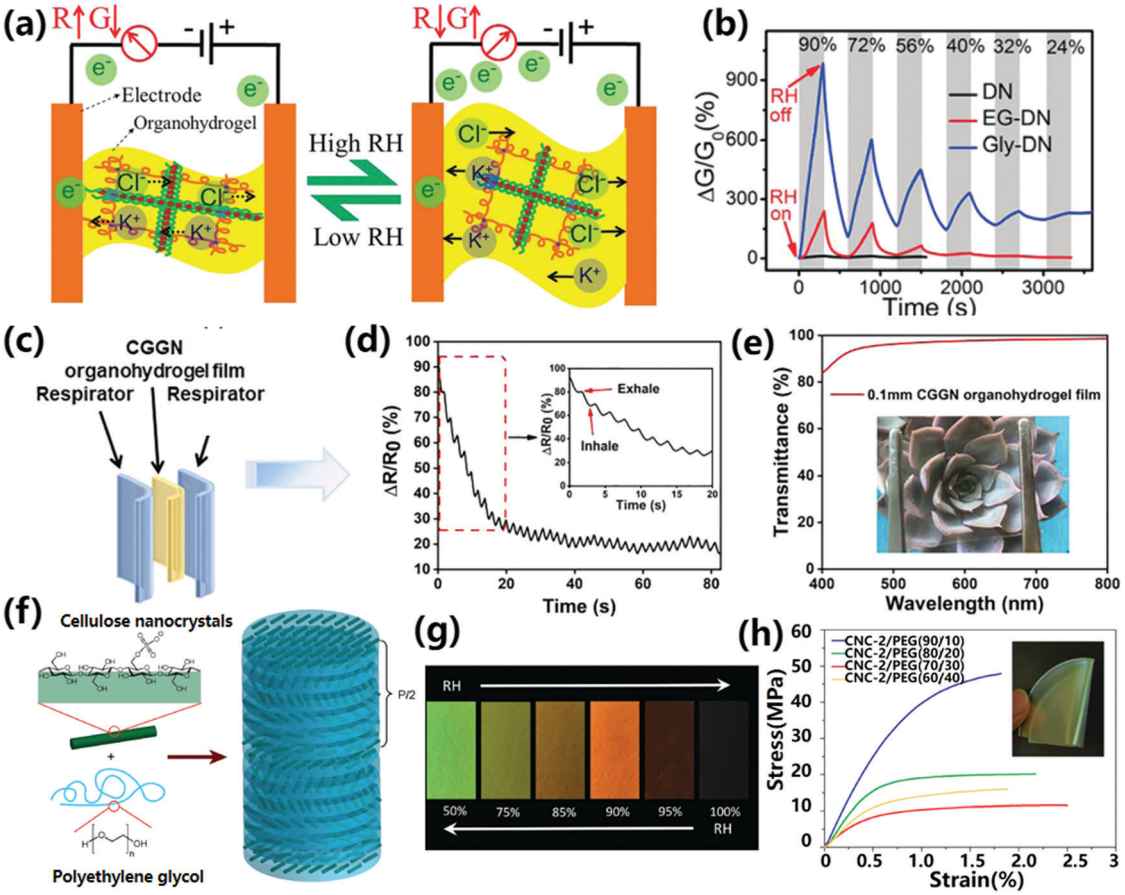

Fig. 10 (a) Schematic illustrating the humidity sensing principle of the organohydrogel. (b) Relative conductivity of DN hydrogels and EG/Gly-DN organic hydrogels in the RH range from 90% to 24% (reprinted with permission from ref. 113 Copyright 2019 The Royal Society of Chemistry). (c) Schematic of a CGGN organohydrogel film clamped between two respirators for facial breath detection. (d) Relative resistance changes of (c) in response to humidity during respiration in 80 seconds. (e) UV-vis spectra of CGGN organohydrogel films with 0.1 mm (reprinted with permission from ref. 67 Copyright 2022 Elsevier). (f) Schematic illustration of the preparation of the CNC/PEG composite. (g) Reversible structure color change diagram of the CNC-2/PEG (80/20) film in the range of 50% to 100% RH under white light illumination. (h) Strain-stress curves of the composite films with different CNC and PEG content were tested at RH 50% (reprinted with permission from ref. 115 Copyright 2017 Wiley).

of all sensors increases immediately. In the detection of 90% RH, the EG-DN and Gly-DN sensors showed responses of 239% and 978%, respectively, corresponding to 19.8 and 80.8 times that of the DN sensor (12.1%). Inspired by the special characteristics of human skin, Ying *et al.* developed an artificial ionic skin (AIskin) with high toughness, stretchability, ambient stability and transparency properties by agarose-polyacrylamide (Agar-PAM).[114] AIskin is a bilayer double-network hydrogel with hygroscopic substances and positively and negatively charged polyelectrolytes in its two separate layers. Zeng *et al.* constructed a starch/PAM dual network through physicochemical crosslinking of starch and *in situ* free-radical polymerization of acrylamide. The sensor prepared by the hydrogel can recognize different expiratory lengths and intensities of human breathing, which may have potential application value in the diagnosis of respiratory diseases.[53]

5.1.2 Other substrates. Gao *et al.* fabricated a chitosan–gelatin–glycerin–NaCl (CGGN) organo-hydrogel film sensor.[67] The transmittance of the 0.1 mm CGGN organo-hydrogel film in the wavelength range of 400 nm to 800 nm could reach up to 98% (Fig. 10e). As shown in Fig. 10c, the CGGN sensor is sandwiched between two respirators (each respirator was made of three layers of non-woven fabric) and then worn on the face for breath detection. In the first 20 s, the dry respirator continuously absorbed the water vapor that exhaled, so the overall resistance trend rapidly decreased. When the water vapor absorbed by the respirator was saturated, the CGGN sensor could stably detect human respiration (Fig. 10d). Pan *et al.* developed a smart ionic skin with PVA, CNFs and $CaCl_2$. The humidity-sensitive ionic skin enables humidity (45–85% RH) sensing and identification *via* chemical and electrical signal transmission.[71]

5.2 Dual-response transparent stretchable humidity sensors

In a dual-response transparent stretchable humidity sensor, when the humidity changes, the electrical resistance of the hydrogel sensor changes, and the transparency/color changes from a transparent to an opaque/colorful state. The humidity sensor has an electrical resistance and transparency response, which can directly monitor the change of humidity. Therefore, the corresponding humidity can be inferred from the visual color or transparency.

5.2.1 PEG-based. Yao *et al.* developed chiral nematic CNC/PEG composite films that result in solid films with a uniform helical structure upon slow drying (Fig. 10f).[115] As the RH increased and decreased from 50% to 100%, the CNC/PEG (80/20 wt%) composite film exhibited reversible swelling and shrinking, so it exhibited a smooth reversible change from green to transparent (Fig. 10g). As shown in Fig. 10h, the specific modulus and specific tensile strength of the CNC-2/PEG composites decreases with the increase of PEG content, and the CNC-2/PEG (90/10 wt%) composite film has a tensile strength of 48.4 ± 8.2 MPa.

5.2.2 PAA-based. Liu *et al.* developed optically transparent and cable-like polyacrylonitrile (PAN)/PAA nanofibres filled with ultrafine fibrils that were obtained *via* electrospinning at a high relative humidity.[116] When the RH decreased from 95% to 45%, the PAN/PAA nanofiber membrane changed from transparent to opaque.

5.3 Brief conclusion

The humidity sensor changes the electrochemical properties of the hydrogel by absorbing H_2O molecules from the hydrophilic group in the hydrogel (Table 4). Such sensors could be used for environmental monitoring as well as human health care activities such as wound healing and breathing.

6. Transparent stretchable gas sensors

Ammonia (NH_3), nitrogen oxides, carbon oxides and other air pollutants are harmful to human and environmental health. Therefore, high sensitivity sensors are required to detect trace amounts of toxic gases in the air. Flexible gas sensors can be comfortably attached to human skin or surfaces, improving the applicability of gas detection. On the other hand, transparent stretchable gas sensors can be combined with transparent devices, such as smart windows,[117–120] to expand their application prospects. Below, we will introduce the latest development of transparent stretchable gas sensors.

Wu *et al.* used a derived ionic conductive PAM/CA double network (DN) hydrogel for the first time and combined it with the organic solvent glycerol (Gly), to prepare a DN-Gly sensor for monitoring NO_2 and NH_3 gases.[121] As shown in Fig. 11a (i, ii, iii), NO_2 molecules can form hydrogen bonds with Gly, PAM and CA

Table 4 Performance of various hydrogels for preparing humidity sensors

Materials	Transmittance (%)	Strain (%)	Stress (KPa)	Humidity-sensing (RH %)	Sensitivity	Self-healing	Antifreeze	Ref.
Eg/Gly-**PAM**/κ-CA	Transparent	1225	—	4–90	0.24 (DN), 6.2 (Eg-DN), 10 (Gly-DN)	Yes	No	113
Agar-**PAM**	81–87%	400	82	13–85	—	Yes	No	114
Starch/**PAM**	Transparent	135	60	35–97	560 (STH-2), 4417 (STH-3)	Yes	No	53
Chitosan–gelatin-glycerin-NaCl	98%	323	2008.2	20–90	2.31	No	No	67
CNFs/PVA/Gly/Ca^{2+}	93.8%	450	590	45–85	0.35	No	Yes	71
CNC/PEG	Transparent ↔ green	2.25	20000	30–100	—	No	No	115
PAN/PAA	Transparent ↔ opaque	≈115	15600	45–95	—	No	No	116

respectively, thus promoting the adsorption of a hydrogel to NO_2 molecules and improving the sensitivity of gas detection. The positive resistance drift of the gas sensor can be explained by the gas blocking mechanism (Fig. 11c). When there is no

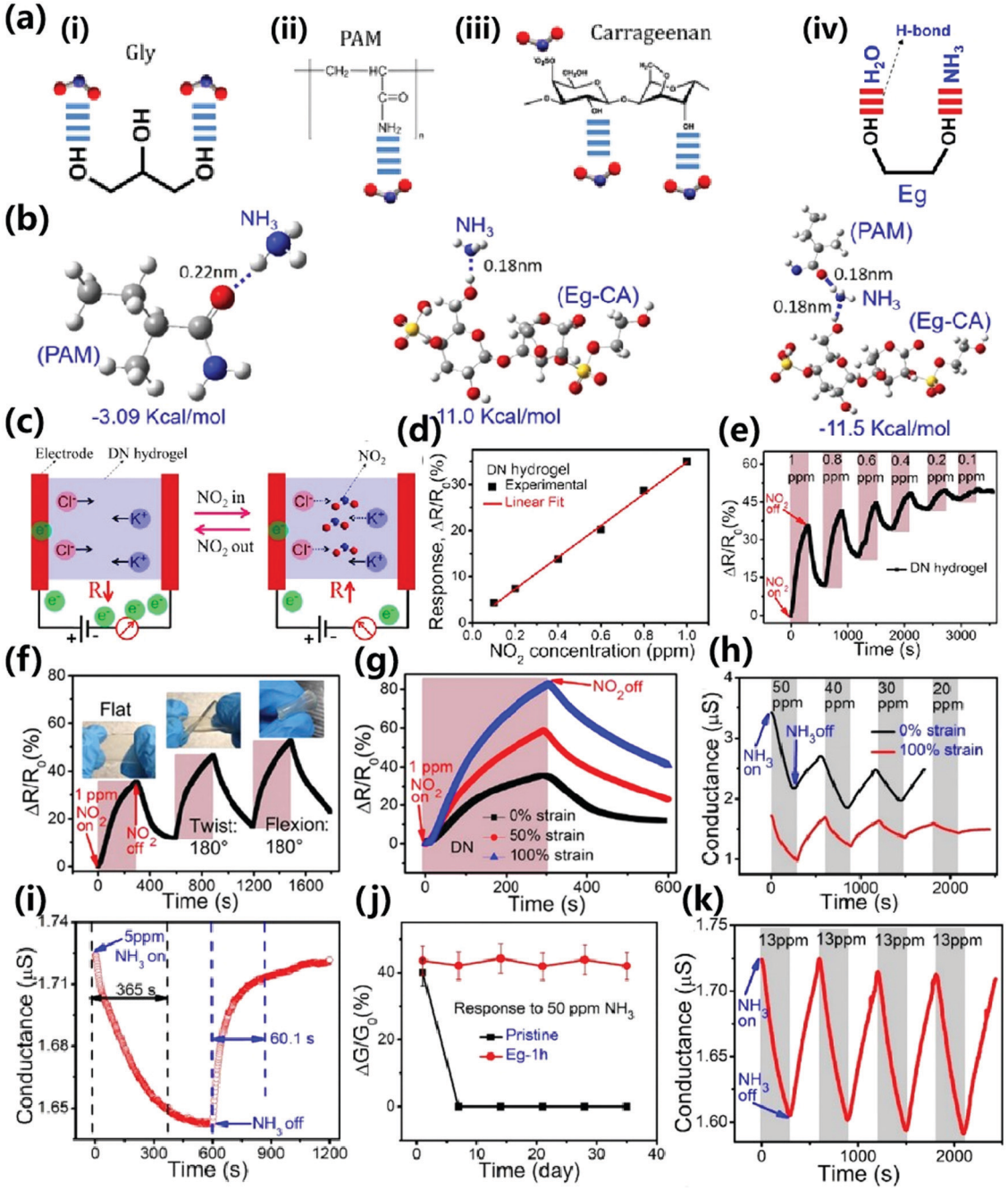

Fig. 11 (a) Schematic diagram of the hydrogen bonds formed between NO_2 molecules and (i) Gly, (ii) PAM and (iii) CA, respectively (reprinted with permission from ref. 121 Copyright 2019 American Chemical Society). (iv) Schematic diagram of hydrogen bonds formed between Eg and H_2O/NH_3 (reprinted with permission from ref. 122 Copyright 2020 American Chemical Society). (b) The optimized interactions between NH_3 and PAM, Eg-CA and Eg-CA/PAM through multiple hydrogen bonds were analyzed using DFT (reprinted with permission from ref. 122 Copyright 2020 American Chemical Society). (c) Diagram of the working mechanism of the NO_2 sensor. (d) Quantitative response of the DN-Gly gas sensor with NO_2 concentration. (e) The relative resistance of the sensor changes as the NO_2 concentration changes from 1 ppm to 0.1 ppm. The shaded part indicates the NO_2 "on" state, and the white part indicates the NO_2 "off" state in the chamber. (f) Dynamic response of DN-Gly hydrogel sensor to NO_2 at a flow rate of 1 ppm in planar, 180° twisted and 180° bent states respectively. (g) The dynamic response of the sensor under different strains at 0.1 ppm NO_2 (reprinted with permission from ref. 121 Copyright 2019 American Chemical Society). (h) The relative resistance of the sensor changes with an NH_3 concentration of 50–20 ppm at 0% and 100% strain. (i) The dynamic curves of sensor response and recovery after NH_3 is turned on and off respectively. (j) The response of the pristine hydrogel sensor and the organic hydrogel sensor to 50 ppm NH_3 varies with the number of days. (k) Real-time response of the sensor to cycle detection of 13 ppm NH_3 (reprinted with permission from ref. 122 Copyright 2020 American Chemical Society).

Table 5 Performance of various hydrogels for preparing gas sensors

Materials	Transmittance (%)	Strain (%)	Stress (KPa)	$\Delta R/R_0$ (%)/gas conc (ppm)	Sensitivity (ppm^{-1})	Self-healing	Antifreeze	Ref.
Gly-CA/PAM	75	1200	—	50.5%/50 (NH_3)	78.5 (NO_2)	—	—	121
Eg-CA/PAM	56	1330	31.8	43.6%/50 (NH_3), 42%/5 (NO_2)	1.4 (NH_3), 8.4 (NO_2)	Yes	Yes −130 °C	122

NH_3/NO_2 gas, K^+ and Cl^- in the hydrogel can move freely and conduct electricity, making the hydrogel have low resistance. When the gas enters, the gas diffuses and dissolves into the hydrogel, which hinders the movement of ions and increases the hydrogel resistance. When the gas is removed again, the dissolved gas in the hydrogel leaves the hydrogel due to the concentration difference and diffuses into the air, and the resistance of the hydrogel returns to the initial value again. As shown in Fig. 11e, as the concentration of NO_2 increases, the number of NO_2 molecules dissolved in the hydrogel increases, so the gas blocking effect increases and the relative resistance of the hydrogel increases, and there is a linear relationship between the concentration and the response of the hydrogel (Fig. 11d). The hydrogel has great mechanical properties, and the sensitivity of the hydrogel gas sensor will not be reduced under various deformations such as flat, bending and stretching (Fig. 11f). As shown in Fig. 11g, with the increase of tensile strain, the relative resistance of the gas sensor increases.

Similarly, Wu *et al.* fabricated transparent, self-healing and freeze-resistant Eg-CA/PAM organic hydrogel gas sensors.[122] They used first-principles density functional theory (DFT) simulation to exploit the analyte and organic hydrogel interactions, as shown in Fig. 11b, NH_3 adsorption energy on PAM and Eg-CA can be higher than on the organic hydrogel adsorption. This indicates that the formation of the double network structure enhances the bonding of NH_3, and the hydrogen bond formed also promotes the adsorption of NH_3 by the organic hydrogel. The hydrogen bond formed between ethylene glycol and water and ammonia can inhibit water evaporation and ice lattice formation, thus giving the hydrogel anti-drying and anti-freezing properties and enhancing the adsorption of gas (Fig. 11a(iv)). As shown in Fig. 11h, the conductance of the gas sensor decreases with the adsorption of NH_3, and is positively correlated with the concentration of NH_3 and negatively correlated with the strain size. The sensor has a great conductivity dynamic response to NH_3. The response time of the sensor is 365 s and the recovery time is 60.1 s when a NH_3 flow of 500 ppm is passed into the gas chamber (Fig. 11i). Organic hydrogels have a good moisturizing effect and stability. The pristine hydrogels lost their sensing ability in a few days, but the conductivity of organic hydrogels decreased significantly in more than 30 days, and the sensing stability is great (Fig. 11j). As shown in Fig. 11k, the organic hydrogel sensor has good stability. When the gas sensor is used for gas detection cycle experiments, the response of the sensor in each cycle is consistent and has good repeatability.

Gas sensors can detect gases as low as a few ppm and increase the resistance of the sensor through the gas blocking effect (Table 5). Although there is little research on gas sensors, we believe that transparent and flexible/scalable gas sensors have very important applications in wearables and healthcare.

7. Conclusions and perspective

This review presents an overview of transparent stretchable hydrogel strain sensors, pressure sensors, temperature sensors, humidity sensors, and gas sensors. The design process, sensing mechanism, performance improvement strategy, and potential sensor applications are summarized. Compared with colored hydrogels, transparent hydrogels have some unique advantages. The response of sensors to different stimuli (such as strain, pressure, temperature and humidity) is closely related to the blocking effect of polymer networks and ion migration rate. However, the principle of the gas sensors is slightly different, and the gas diffuses and dissolves into the hydrogel, thus preventing the movement of ions. The transparent stretchable wearable strain sensors can be attached to the skin to monitor various human movements and tiny physiological signals in real-time. In addition, when it acts on the human–computer interaction interface, it completes the exchange of information or sends instructions to the system. The transparent flexible pressure sensors can monitor slight pressure such as raindrops and large pressure like cars. It also functions as sensor arrays and an intelligent touchscreen. The temperature sensors prompt disease diagnosis and early warning to avoid accidents and provide information about the surrounding environment. The humidity sensors can continuously detect human respiration and ambient humidity and make humidity alarms. The gas sensors can detect the concentration of harmful gases, which is of great significance to air quality and human health.

Although transparent stretchable hydrogels are widely used in various sensors, some challenges are still present. Firstly, there are some limitations in the choice of substrates and additives for transparent hydrogel sensors, and the more the additives, the worse the transparency. Secondly, the hydrogel prepared should have more functions at the same time, such as antifreeze, anti-dryness, self-healing, *etc.*, and can be committed to double sensing or multiple sensing, and the detection of different stimulus signals in multiple sensing should avoid mutual interference, to make it more suitable for human life. Thirdly, the materials used to prepare hydrogel sensors need to be more non-toxic, pollution-free, biocompatible and degradable. Moreover, the prepared hydrogel sensor requires higher transmittance and better mechanical properties. Fourthly, hydrogel sensors with inevitable ionic conduction suffer from inconsistent resistance changes over time under direct current (DC) due to the ion-derived migration and the formation of an

electric double layer, which affects the stability of the sensor.[123] Compared with the DC test mode, the alternating current (AC) test mode is more suitable for ionic conductive hydrogel-based sensors. When the hydrogel sensor is connected to the AC power supply, the cathode and anode are repeatedly reversed, and the ions are continuously diffused and moved inside the hydrogel, thus reducing the chance of forming a double electric layer at the two poles, and the circuit shows negligible capacitance in the resting state.[124,125] Therefore, AC as the power supply equipment of the hydrogel sensor is a better choice. And then, the development of hydrogel sensors to automation and intelligence is a promising research direction. These include hydrogel drivers, artificial intelligence, human–computer interaction, hydrogel generators, energy storage and conversion. Finally, more research and exploration are needed to further improve the sensitivity, circularity, stability and repeatability of hydrogel sensors.

Transparent stretchable hydrogel sensors have strong interdisciplinary characteristics, and the joint efforts of multiple disciplines are needed to further improve the performance and function of hydrogel and sensors. We hope to speed up the development of hydrogel sensors by reviewing the latest progress and opening up new paths for many new fields. For example, wearable transparent hydrogel sensors on soft robots can be perceived when interacting with the surrounding environment, which provides a new idea for developing wearable sensors integrated with soft robot systems. Optical devices based on transparent hydrogels have good transparency and flexural properties. By changing the local refractive index of materials, they can be used as the preferred materials for liquid crystal zoom lenses. In addition, transparent hydrogel sensors are considered energy storage devices that can continuously power the next generation of wearable electronics.

Conflicts of interest

There are no conflicts to declare.

Acknowledgements

This research was supported by the Science Foundation of China University of Petroleum, Beijing (No. 2462019BJRC007, 2462020YXZZ018) and the National Natural Science Foundation of China (No. 5211101820).

References

1 G.-H. Zhang, L. Zhang, Q.-H. Zhu, H. Chen, W.-L. Yuan, J. Fu, S.-L. Wang, L. He and G.-H. Tao, *ACS Mater. Lett.*, 2021, **4**, 136–144.
2 D. Wang, X. Li, H. Tian, X. Chen, B. Nie, Y. Luo and J. Shao, *Appl. Mater. Today*, 2021, **25**, 101247.
3 L. Liang, H. Lv, X. L. Shi, Z. Liu, G. Chen, Z. G. Chen and G. Sun, *Mater. Horiz.*, 2021, **8**, 2750–2760.
4 C. Cui, C. Y. Shao, L. Meng and J. Yang, *ACS Appl. Mater. Interfaces*, 2019, **11**, 39228–39237.
5 L. Liu, S. Niu, J. Zhang, Z. Mu, J. Li, B. Li, X. Meng, C. Zhang, Y. Wang, T. Hou, Z. Han, S. Yang and L. Ren, *Adv. Mater.*, 2022, 2200823, DOI: **10.1002/adma.202200823**.
6 M. Li, S. Chen, B. Fan, B. Wu and X. Guo, *Adv. Funct. Mater.*, 2020, **30**, 2003214.
7 Z. Wu, L. Wei, S. Tang, Y. Xiong, X. Qin, J. Luo, J. Fang and X. Wang, *ACS Nano*, 2021, **15**, 18880–18894.
8 M. Amit, L. Chukoskie, A. J. Skalsky, H. Garudadri and T. N. Ng, *Adv. Funct. Mater.*, 2019, **30**, 1905241.
9 Z. Cao, Y. Yang, Y. Zheng, W. Wu, F. Xu, R. Wang and J. Sun, *J. Mater. Chem. A*, 2019, **7**, 25314–25323.
10 J. H. Lee, H. Chen, E. Kim, H. Zhang, K. Wu, H. Zhang, X. Shen, Q. Zheng, J. Yang, S. Jeon and J. K. Kim, *Mater. Horiz.*, 2021, **8**, 1488–1498.
11 E. Singh, M. Meyyappan and H. S. Nalwa, *ACS Appl. Mater. Interfaces*, 2017, **9**, 34544–34586.
12 H. Zhao, R. Su, L. Teng, Q. Tian, F. Han, H. Li, Z. Cao, R. Xie, G. Li, X. Liu and Z. Liu, *Nanoscale*, 2022, **14**, 1653–1669.
13 Q. Wu, Y. Qiao, R. Guo, S. Naveed, T. Hirtz, X. Li, Y. Fu, Y. Wei, G. Deng, Y. Yang, X. Wu and T. L. Ren, *ACS Nano*, 2020, **14**, 10104–10114.
14 T. H. Park, S. Yu, S. H. Cho, H. S. Kang, Y. Kim, M. J. Kim, H. Eoh, C. Park, B. Jeong, S. W. Lee, D. Y. Ryu, J. Huh and C. Park, *NPG Asia Mater.*, 2018, **10**, 328–339.
15 C. H. Lee and R. MacKinnon, *Cell*, 2019, **179**, 1582–1589.
16 N. Jo, B. Kim, S. M. Lee, J. Oh, I. H. Park, K. Jin Lim, J. S. Shin and K. H. Yoo, *Biosens. Bioelectron.*, 2018, **102**, 164–170.
17 Y. Zhou, X. Dong, Y. Mi, F. Fan, Q. Xu, H. Zhao, S. Wang and Y. Long, *J. Mater. Chem. A*, 2020, **8**, 10007–10025.
18 X. Liu, J. Liu, S. Lin and X. Zhao, *Mater. Today*, 2020, **36**, 102–124.
19 X. Luo, L. Zhu, Y. C. Wang, J. Li, J. Nie and Z. L. Wang, *Adv. Funct. Mater.*, 2021, **31**, 2104928.
20 B. Sui, Y. Zhang, L. Huang, Y. Chen, D. Li, Y. Li and B. Yang, *ACS Sustainable Chem. Eng.*, 2020, **8**, 18492–18499.
21 Q. Ding, X. Xu, Y. Yue, C. Mei, C. Huang, S. Jiang, Q. Wu and J. Han, *ACS Appl. Mater. Interfaces*, 2018, **10**, 27987–28002.
22 Z. Yang, L. Chen, D. J. McClements, C. Qiu, C. Li, Z. Zhang, M. Miao, Y. Tian, K. Zhu and Z. Jin, *Food Hydrocolloids*, 2022, **124**, 107218.
23 L. Wang, T. Xu and X. Zhang, *TrAC, Trends Anal. Chem.*, 2021, **134**, 116130.
24 L. Meng, A. P. F. Turner and W. C. Mak, *Biotechnol. Adv.*, 2020, **39**, 107398.
25 S. Mirjalali, S. Peng, Z. Fang, C. H. Wang and S. Wu, *Adv. Mater. Technol.*, 2021, **7**, 2100545.
26 X. J. Pei, H. Zhang, Y. Zhou, L. J. Zhou and J. Fu, *Mater. Horizons*, 2020, **7**, 1872–1882.
27 Z. Yang, R. Huang, B. Zheng, W. Guo, C. Li, W. He, Y. Wei, Y. Du, H. Wang, D. Wu and H. Wang, *Adv. Sci.*, 2021, **8**, 2003627.

28 X. Qu, S. Wang, Y. Zhao, H. Huang, Q. Wang, J. Shao, W. Wang and X. Dong, *Chem. Eng. J.*, 2021, **425**, 131523.
29 J. Qu, X. Zhao, Y. Liang, T. Zhang, P. X. Ma and B. Guo, *Biomaterials*, 2018, **183**, 185–199.
30 H. Chen, C. Peng, L. Wang, X. Li, M. Yang, H. Liu, H. Qin and W. Chen, *Chem. Eng. J.*, 2021, **403**, 126341.
31 Z. Qiao, M. Cao, K. Michels, L. Hoffman and H.-F. Ji, *Polym. Rev.*, 2019, **60**, 420–441.
32 K. Chen, Y. Feng, Y. Zhang, L. Yu, X. Hao, F. Shao, Z. Dou, C. An, Z. Zhuang, Y. Luo, Y. Wang, J. Wu, P. Ji, T. Chen and H. Wang, *ACS Appl. Mater. Interfaces*, 2019, **11**, 36458–36468.
33 X. Du, J. Zhai, X. Li, Y. Zhang, N. Li and X. Xie, *ACS Sens.*, 2021, **6**, 1990–2001.
34 H. Lü, L. Yang, Y. Zhou, R. Qu, Y. Xu, S. Shang and N. Hui, *J. Electrochem. Soc.*, 2021, **168**, 047506.
35 X. Zheng, Y. Gao, X. Ren and G. Gao, *J. Mater. Chem. C*, 2021, **9**, 3343–3351.
36 Y. Gao, Y. Wang, S. Xia and G. Gao, *Sci. China Mater.*, 2021, **64**, 2313–2324.
37 G. Su, J. Cao, X. Zhang, Y. Zhang, S. Yin, L. Jia, Q. Guo, X. Zhang, J. Zhang and T. Zhou, *J. Mater. Chem. A*, 2020, **8**, 2074–2082.
38 C.-Y. Lo, Y. Zhao, C. Kim, Y. Alsaid, R. Khodambashi, M. Peet, R. Fisher, H. Marvi, S. Berman, D. Aukes and X. He, *Mater. Today*, 2021, **50**, 35–43.
39 X. Liu, Q. Zhang and G. Gao, *ACS Nano*, 2020, **14**, 13709–13717.
40 J. Wei, F. Wan, P. Zhang, Z. Zeng, H. Ping, J. Xie, Z. Zou, W. Wang, H. Xie, Z. Shen, L. Lei and Z. Fu, *Chem. Eng. J.*, 2021, **424**, 130549.
41 Q. Wang, M. Jian, C. Wang and Y. Zhang, *Adv. Funct. Mater.*, 2017, **27**, 1605657.
42 H. Guo, C. Lan, Z. Zhou, P. Sun, D. Wei and C. Li, *Nanoscale*, 2017, **9**, 6246–6253.
43 G. Ye, Z. Song, T. Yu, Q. Tan, Y. Zhang, T. Chen, C. He, L. Jin and N. Liu, *ACS Appl. Mater. Interfaces*, 2020, **12**, 1486–1494.
44 H. Gong, Z. Xu, Y. Yang, Q. Xu, X. Li, X. Cheng, Y. Huang, F. Zhang, J. Zhao, S. Li, X. Liu, Q. Huang and W. Guo, *Biosens. Bioelectron.*, 2020, **169**, 112567.
45 L. Zhang, J. Wang, S. Wang, L. Wang and M. Wu, *J. Mater. Chem. C*, 2022, **10**, 4327–4335.
46 Z. Chen, Y. Chen, M. S. Hedenqvist, C. Chen, C. Cai, H. Li, H. Liu and J. Fu, *J. Mater. Chem. B*, 2021, **9**, 2561–2583.
47 Q. Zhang, X. Liu, L. J. Duan and G. H. Gao, *Chem. Eng. J.*, 2019, **365**, 10–19.
48 H. Huang, L. Han, J. Li, X. Fu, Y. Wang, Z. Yang, X. Xu, L. Pan and M. Xu, *J. Mater. Chem. A*, 2020, **8**, 10291–10300.
49 C. C. Kim, H. H. Lee, K. H. Oh and J. Y. Sun, *Science*, 2016, **353**, 682–687.
50 X. Guo, F. Yang, W. Liu, C. Han and R. Wang, *J. Mater. Chem. A*, 2021, **9**, 14806–14817.
51 H. Yu, Y. Tian, M. Dirican, D. Fang, C. Yan, J. Xie, D. Jia, Y. Liu, C. Li, M. Cui, H. Liu, G. Chen, X. Zhang and J. Tao, *Carbohydr. Polym.*, 2021, **273**, 118539.
52 J. Yan, Y. Xia, J. Lai, C. Zhao, D. Xiang, H. Li, Y. Wu, Z. Li and H. Zhou, *Macromol. Mater. Eng.*, 2022, **307**, 2100765.
53 S. Zeng, J. Zhang, G. Zu and J. Huang, *Carbohydr. Polym.*, 2021, **267**, 118198.
54 Z. Wu, W. Shi, H. Ding, B. Zhong, W. Huang, Y. Zhou, X. Gui, X. Xie and J. Wu, *J. Mater. Chem. C*, 2021, **9**, 13668–13679.
55 Z. Li, Z. Wu, H. Ding, Y. Wei, X. Yang, J. Wu and K. Tao, presented in part at the 2021 21st International Conference on Solid-State Sensors, Actuators and Microsystems (Transducers), 2021.
56 S. M. Kim, H. J. Kim, H. J. Jung, J. Y. Park, T. J. Seok, Y. H. Choa, T. J. Park and S. W. Lee, *Adv. Funct. Mater.*, 2018, **29**, 1807760.
57 G. Li, C. Li, G. Li, D. Yu, Z. Song, H. Wang, X. Liu, H. Liu and W. Liu, *Small*, 2022, **18**, 2101518.
58 H. Wang, Z. Li, Z. Liu, J. Fu, T. Shan, X. Yang, Q. Lei, Y. Yang and D. Li, *J. Mater. Chem. C*, 2022, **10**, 1594–1605.
59 Z. Wu, X. Yang and J. Wu, *ACS Appl. Mater. Interfaces*, 2021, **13**, 2128–2144.
60 H. Zhi, J. Gao and L. Feng, *ACS Sens.*, 2020, **5**, 772–780.
61 Q. Jiao, L. Cao, Z. Zhao, H. Zhang, J. Li and Y. Wei, *Biomacromolecules*, 2021, **22**, 1220–1230.
62 B. Zhao, Q. Chen, G. Da, J. Yao, Z. Shao and X. Chen, *J. Mater. Chem. C*, 2021, **9**, 8955–8965.
63 J. Mao, C. Zhao, L. Liu, Y. Li, D. Xiang, Y. Wu and H. Li, *Compos. Commun.*, 2021, **25**, 100733.
64 X. Jing, H. Li, H.-Y. Mi, Y.-J. Liu, P.-Y. Feng, Y.-M. Tan and L.-S. Turng, *Sens. Actuators, B*, 2019, **295**, 159–167.
65 Z. Wu, H. Ding, K. Tao, Y. Wei, X. Gui, W. Shi, X. Xie and J. Wu, *ACS Appl. Mater. Interfaces*, 2021, **13**, 21854–21864.
66 B. W. Yang and W. Yuan, *ACS Appl. Mater. Interfaces*, 2019, **11**, 16765–16775.
67 Y. Gao, F. Jia and G. Gao, *Chem. Eng. J.*, 2022, **430**, 132919.
68 Q. Wang, H. Ding, X. Hu, X. Liang, M. Wang, Q. Liu, Z. Li and G. Sun, *Mater. Horizons*, 2020, **7**, 2673–2682.
69 H. Charaya, T. G. La, J. Rieger and H. J. Chung, *Adv. Mater. Technol.*, 2019, **4**, 1900327.
70 Q. Chang, Y. He, Y. Liu, W. Zhong, Q. Wang, F. Lu and M. Xing, *Adv. Funct. Mater.*, 2020, **30**, 1910080.
71 X. Pan, Q. Wang, R. Guo, S. Cao, H. Wu, X. Ouyang, F. Huang, H. Gao, L. Huang, F. Zhang, L. Chen, Y. Ni and K. Liu, *J. Mater. Chem. A*, 2020, **8**, 17498–17506.
72 J. Song, S. Chen, L. Sun, Y. Guo, L. Zhang, S. Wang, H. Xuan, Q. Guan and Z. You, *Adv. Mater.*, 2020, **32**, 1906994.
73 Z. Li, S. Zhang, Y. Chen, H. Ling, L. Zhao, G. Luo, X. Wang, M. C. Hartel, H. Liu and Y. Xue, *Adv. Funct. Mater.*, 2020, **30**, 2003601.
74 K. Chen, M. Liu, F. Wang, Y. Hu, P. Liu, C. Li, Q. Du, Y. Yu, X. Xiao and Q. Feng, *Front. Bioeng. Biotechnol.*, 2022, **10**, 846401.
75 S. Zhang, Y. Zhang, B. Li, P. Zhang, L. Kan, G. Wang, H. Wei, X. Zhang and N. Ma, *ACS Appl. Mater. Interfaces*, 2019, **11**, 32441–32448.

76 S. Pan, M. Xia, H. Li, X. Jiang, P. He, Z. Sun and Y. Zhang, *J. Mater. Chem. C*, 2020, **8**, 2827–2837.
77 G. Ge, Y. Zhang, J. Shao, W. Wang, W. Si, W. Huang and X. Dong, *Adv. Funct. Mater.*, 2018, **28**, 1802576.
78 Y. Yu, X. Zhao and L. Ye, *Appl. Surf. Sci.*, 2021, **562**, 150162.
79 H. Lin, Y. Fu, Y. Gao and A. Mo, *Macromol. Mater. Eng.*, 2020, **305**, 2000064.
80 M. You, Q. Li, S. Zhang, D. Wu, H. Qin, Y. Wang, W. Wen, W. He and H. Liu, *Radiat. Phys. Chem.*, 2021, **189**, 109757.
81 S. Fan, Q. Tang, J. Wu, D. Hu, H. Sun and J. Lin, *J. Mater. Sci.*, 2008, **43**, 5898–5904.
82 J. Xu, R. Jing, X. Ren and G. Gao, *J. Mater. Chem. A*, 2020, **8**, 9373–9381.
83 X. Zhang, N. Sheng, L. Wang, Y. Tan, C. Liu, Y. Xia, Z. Nie and K. Sui, *Mater. Horizons*, 2019, **6**, 326–333.
84 F. Ji, M. Jiang, Q. Yu, X. Hao, Y. Zhang, J. Zhu, S. Luo and J. Li, *Front. Chem.*, 2021, **9**, 758844.
85 Y. Peng, B. Yan, Y. Li, J. Lan, L. Shi and R. Ran, *J. Mater. Sci.*, 2019, **55**, 1280–1291.
86 J. Yang, Q. Kang, B. Zhang, X. Fang, S. Liu, G. Qin and Q. Chen, *Mater. Sci. Eng., C*, 2021, **130**, 112452.
87 B. Li, L. Kan, C. Li, W. Li, Y. Zhang, R. Li, H. Wei, X. Zhang and N. Ma, *J. Mater. Chem. C*, 2021, **9**, 1044–1050.
88 X. Qu, Y. Zhao, Z. Chen, S. Wang, Y. Ren, Q. Wang, J. Shao, W. Wang and X. Dong, *Research*, 2021, **2021**, 9845482.
89 M. Ma, Y. Shang, H. Shen, W. Li and Q. Wang, *Chem. Eng. J.*, 2021, **420**, 129865.
90 Q. H. Wang, X. F. Pan, C. M. Lin, X. J. Ma, S. L. Cao and Y. H. Ni, *Chem. Eng. J.*, 2020, **396**, 125341.
91 W. Ma, W. Cao, T. Lu, Z. Jiang, R. Xiong, S. K. Samal and C. Huang, *ACS Appl. Mater. Interfaces*, 2021, **13**, 58048–58058.
92 M. Wu, J. Chen, Y. Ma, B. Yan, M. Pan, Q. Peng, W. Wang, L. Han, J. Liu and H. Zeng, *J. Mater. Chem. A*, 2020, **8**, 24718–24733.
93 G. Gu, H. Xu, S. Peng, L. Li, S. Chen, T. Lu and X. Guo, *Soft Robot.*, 2019, **6**, 368–376.
94 Y. Lee, S. H. Cha, Y. W. Kim, D. Choi and J. Y. Sun, *Nat. Commun.*, 2018, **9**, 1804.
95 X. Y. Yin, Y. Zhang, J. Xiao, C. Moorlag and J. Yang, *Adv. Funct. Mater.*, 2019, **29**, 1904716.
96 F. Mo, Y. Huang, Q. Li, Z. Wang, R. Jiang, W. Gai and C. Zhi, *Adv. Funct. Mater.*, 2021, **31**, 2010830.
97 C.-C. Kim, H.-H. Lee, K. H. Oh and J.-Y. Sun, *Science*, 2016, **353**, 682–687.
98 M. Sarwar, Y. Dobashi, E. Glitz, M. Farajollahi and J. Madden, *Proc. SPIE*, 2015, **9430**, 943026–943034.
99 X. Guo, F. Yang, W. Liu, C. Han, Y. Bai, X. Sun, L. Hao, W. Jiao and R. Wang, *J. Mater. Chem. A*, 2021, **9**, 14806–14817.
100 J. Wu, Z. X. Wu, Y. M. Wei, H. J. Ding, W. X. Huang, X. C. Gui, W. X. Shi, Y. Shen, K. Tao and X. Xie, *ACS Appl. Mater. Interfaces*, 2020, **12**, 19069–19079.
101 J. Wu, S. J. Han, T. Z. Yang, Z. Li, Z. X. Wu, X. C. Gui, K. Tao, J. M. Miao, L. K. Norford, C. Liu and F. W. Huo, *ACS Appl. Mater. Interfaces*, 2018, **10**, 19097–19105.
102 Y. Wang, L. Zhang and A. Lu, *J. Mater. Chem. A*, 2020, **8**, 13935–13941.
103 J. Wen, J. Tang, H. M. Ning, N. Hu, Y. Y. Zhu, Y. K. Gong, C. H. Xu, Q. N. Zhao, X. P. Jiang, X. L. Hu, L. Lei, D. Wu and T. Huang, *Adv. Funct. Mater.*, 2021, **31**, 2011176.
104 D. Grifoni, L. Bacci, G. Zipoli, L. Albanese and F. Sabatini, *Dyes Pigm.*, 2011, **91**, 279–285.
105 R. Wang, X. Wang, Y. Zhan, Z. Xu, Z. Xu, X. Feng, S. Li and H. Xu, *ACS Appl. Mater. Interfaces*, 2019, **11**, 37502–37512.
106 H. Wei, Z. Wang, H. Zhang, Y. Huang, Z. Wang, Y. Zhou, B. B. Xu, S. Halila and J. Chen, *Chem. Mater.*, 2021, **33**, 6731–6742.
107 Y. Hu, M. Zhang, C. Qin, X. Qian, L. Zhang, J. Zhou and A. Lu, *Carbohydr. Polym.*, 2021, **265**, 118078.
108 Q. Y. Chen, H. Tang, J. L. Liu, R. R. Wang, J. Sun, J. R. Yao, Z. Z. Shao and X. Chen, *Chem. Eng. J.*, 2021, **422**, 130091.
109 Z. Zhang, T. Chao and S. Jiang, *J. Phys. Chem. B*, 2008, **112**, 5327.
110 C. Zhang, Y. S. Zhou, H. J. Han, H. X. Zheng, W. H. Xu and Z. K. Wang, *ACS Nano*, 2021, **15**, 1785–1794.
111 X. F. Shi and P. Y. Wu, *Small*, 2021, **17**, 2101220.
112 S. Choi, Y. Eom, S. M. Kim, D. W. Jeong, J. Han, J. M. Koo, S. Y. Hwang, J. Park and D. X. Oh, *Adv. Mater.*, 2020, **32**, 1907064.
113 J. Wu, Z. X. Wu, H. H. Xu, Q. Wu, C. Liu, B. R. Yang, X. C. Gui, X. Xie, K. Tao, Y. Shen, J. M. Miao and L. K. Norford, *Mater. Horizons*, 2019, **6**, 595–603.
114 B. Ying, Q. Wu, J. Li and X. Liu, *Mater. Horizons*, 2020, **7**, 477–488.
115 K. Yao, Q. Meng, V. Bulone and Q. Zhou, *Adv. Mater.*, 2017, **29**, 1701323.
116 Y. Liu, Y. Liu, J.-H. Lee, C. Lee, M. Park and H.-Y. Kim, *Compos. Sci. Technol.*, 2015, **117**, 404–409.
117 Y. Zhou, S. Wang, J. Peng, Y. Tan, C. Li, F. Y. C. Boey and Y. Long, *Joule*, 2020, **4**, 2458–2474.
118 S. Wang, T. Jiang, Y. Meng, R. Yang, G. Tan and Y. Long, *Science*, 2021, **374**, 1501–1504.
119 Y. Zhou, F. Fan, Y. Liu, S. Zhao, Q. Xu, S. Wang, D. Luo and Y. Long, *Nano Energy*, 2021, **90**, 106613.
120 Y. Niu, Y. Zhou, D. Du, X. Ouyang, Z. Yang, W. Lan, F. Fan, S. Zhao, Y. Liu, S. Chen, J. Li and Q. Xu, *Adv. Sci.*, 2022, **6**, 2105184.
121 J. Wu, Z. X. Wu, S. J. Han, B. R. Yang, X. C. Gui, K. Tao, C. Liu, J. M. Miao and L. K. Norford, *ACS Appl. Mater. Interfaces*, 2019, **11**, 2364–2373.
122 J. Wu, Z. Wu, W. Huang, X. Yang, Y. Liang, K. Tao, B. R. Yang, W. Shi and X. Xie, *ACS Appl. Mater. Interfaces*, 2020, **12**, 52070–52081.
123 Y. Zhao, B. Zhang, B. Yao, Y. Qiu, Z. Peng, Y. Zhang, Y. Alsaid, I. Frenkel, K. Youssef, Q. Pei and X. He, *Matter*, 2020, **3**, 1196–1210.
124 Z. Lei and P. Wu, *Nat. Commun.*, 2019, **10**, 3429.
125 Y. Ye, Y. Zhang, Y. Chen, X. Han and F. Jiang, *Adv. Funct. Mater.*, 2020, **30**, 2003430.